Journal of Sound and Vibration 564 (2023) 117799

Contents lists available at ScienceDirect

Journal of Sound and Vibration

journal homepage: www.elsevier.com/locate/jsvi

The prototype, mathematical model, sensitivity analysis and preliminary control strategy for Adaptive Tuned Particle Impact Damper

Mateusz Żurawski [a,*], Cezary Graczykowski [b], Robert Zalewski [a]

[a] Institute of Machine Design Fundamentals, Warsaw University of Technology, Warsaw, Poland
[b] Institute of Fundamental Technological Research, Polish Academy of Sciences, Warsaw, Poland

ARTICLE INFO

Keywords:
Adaptive Tuned Particle Impact Damper
Damping of vibrations
Semi-active damping
Controllable damper
Control function
Sensitivity analysis
System optimization
Real-time control strategy

ABSTRACT

The paper presents a novel approach for prototyping and modelling of the Adaptive Tuned Particle Impact Damper (ATPID). After introducing the operation and potential disadvantages of the classical Particles Impact Dampers (PIDs) the authors propose the concept of single-grain controllable damper, which can adapt to actual dynamic excitation by a real-time change of the container height. The investigations focus on the methodology of simplified mathematical modelling of the ATPID damper based on grain physical properties, nonlinear soft contact theory, and control function of the absorber height being a novel component used to optimize dynamic response of the system. The proposed ATPID model is positively verified against the experimental results obtained from the developed test stand including a vibrating beam equipped with the proposed innovative attenuator. The conducted analyses clearly reveal the operating principles of the ATPID damper, the types of grain movement, the influence of shock absorber parameters on the vibrating system response and the energy balance of the system. The solution of the formulated optimization problem aimed at minimization of vibration amplitudes allows to find the optimal damper height for various physical parameters of the grain and the external excitation and to achieve a high efficiency of the proposed damper reaching 90%. In addition, a real-time control strategy providing adaptation of the ATPID damper to changing amplitude of kinematic excitation and effective mitigation of steady-state vibrations is proposed and verified experimentally.

1. Introduction

Mitigation of vibrations has been a popular field of theoretical and experimental research for many years. A literature review reveals that a lot of different technical solutions based on various physical phenomena can be developed [1]. One interesting example is a Particles Impact Damper (PID). Such a device is composed of a container filled with granular material and it is characterized by a passive damping ability resulting from non-elastic grain–grain and grain–container collisions. The energy dissipation process is based on a transfer of momentum between PID elements and the change of their kinetic energy into heat via the combined effects of inelastic collisions and frictional losses. The physical properties of applied particles, which strongly influence damping efficiency, are resistant to impact of heat and resulting changes of temperature. This allows to effectively apply PIDs to damp vibrations of technical systems operating in harsh environments, where standard viscous absorbers fail.

* Corresponding author.
E-mail addresses: Mateusz.Zurawski@pw.edu.pl (M. Żurawski), Cezary.Graczykowski@ippt.pan.pl (C. Graczykowski), Robert.Zalewski@pw.edu.pl (R. Zalewski).

https://doi.org/10.1016/j.jsv.2023.117799
Received 14 April 2022; Received in revised form 22 March 2023; Accepted 17 May 2023
Available online 24 May 2023

The current research on Particle Impact Dampers can be divided into two main branches [2]:

– experimental research aimed at modification of the standard and development of novel PID constructions [3–5], determination of their damping characteristics [6–8] and analysis of the influence of physical, geometrical and excitation parameters on PIDs efficiency [9–11],

– mathematical modelling of PID absorbers and simulation of their response to the dynamic excitation using physical models based on a soft contact theory [12,13], hard contact theory [2,14] and Leidefrost effect [15,16].

The main problem in Particle Impact Damper simulations is proper modelling of the collisions between grains of the applied granular material. Kruggel–Emden et al. [17] present a review of the normal force models which can be divided into the following categories: linear [18], partly nonlinear [19], fully nonlinear [20–22] and hysteretic [23]. Linear and nonlinear viscoelastic collision models were described by Lee– Hermann [19], Kuwabara–Kono [24] and others who defined contact forces using reduced stiffness and damping coefficients based on physical and geometrical parameters of grains. The hysteretic model [23] was used to include plasticity effects in grains collisions. The hard contact model is defined by new initial conditions imposed on the velocities of the particle after impact using the restitution coefficient. The authors of [15] describe a novel PID modelling method, in which one part of grains is considered as a gas flow with a low Reynolds number and the second part is treated as a solid-state. Such an approach allows extending the standard contact force model to the model with a changeable damping coefficient which depends on grains and system parameters. Such a modelling approach is called by granullar Leidenfrost effect.

To reflect the effects of the collisions between grains in classical particles impact damper construction the authors of the papers [25–28] propose a reduced system of the multiple colliding particles by the model of the 1–DOF and 2–DOF systems with equivalent parameters such as connection stiffness, mass ratio and recovery coefficient. Moreover, the impacts are described by the law of conservation of momentum and the rolling friction is introduced to the reduced grains. The proposed methods are validated by experimental research and obtained results show the effectiveness of the damping ability in practical applications.

One of the most interesting aspects of mathematical analysis of Particle Impact Dampers are methods aimed at optimization of their parameters. Genetic Algorithms were used in paper [29] to optimize an enclosure height, grain mass and coefficient of restitution to maximize the value of the loss factor. In paper [30] the authors optimize a PID damping effect using bound optimization by quadratic approximation (BOBYQA) to obtain minimum–maximum amplitude (MMA) of vibrations and minimum total vibration level (MTVL). Another interesting example of parameters optimization is presented in [31] where the problem is finding the best locations of the damper on the tested plate and the most effective container volume filling ratio. For this approach, the Swarm Algorithm was used for the optimization process.

From the vibration mitigation point of view, the operation of PID is reflected in the decreased amplitudes of system vibrations, mostly in a resonance range of excitation. In some cases, this effect can be considered similar to the effect of a Tuned Mass Damper (TMD). The papers [32,33] compare the impact of both devices on the damping of vibrations. The authors also propose modelling of both absorbers as single or multi degree of freedom systems with similar operation principles.

Regarding PID applications Junling et al. [34] describe an example of using PID in wind turbines to absorb tower vibrations. Another field of application is automotive environment. In [35] the authors describe experimental and numerical studies verifying the possibility of using PID to damp vibrations and increase a riding comfort of a dump truck. An interesting approach is presented in [36], where the authors use PID to absorb saw oscillations and gear vibrations [37]. PIDs can be potentially used in large constructions such as high-rise buildings, which are often exposed to seismic excitations and significant dynamic loads. Experimental and theoretical studies regarding vibrations attenuations of such structures are described in [38,39].

The mentioned papers are only a part of the world literature. A lot of articles related to different approaches to modelling, simulation and optimization of phenomena occurring inside PIDs can be referenced. However, a few of these analyses allows for a modification of damper parameters during a vibration mitigation process. For this reason, the authors focus on the proposed in previous papers [40,41] a new concept of PID assuming the possibility of dynamic tuning. The proposed damper is called Adaptive Tuned Particle Impact Damper (ATPID) and enables control of the selected damper parameter (height of the container) during the process of vibrations damping. The paper [42] describes active parameter control of the impact damper. Despite many similarities between the considered impact damper and the ATPID absorber, there are significant differences in the dynamics of these systems. In both cases, different assumptions concerning the movement of the considered system are made and different corresponding numerical analyses are performed. This leads to a different description of the principle of the auxiliary mass optimal behaviour, which corresponds to the most effective process of vibration damping. The semi-active control algorithm presented in the paper [42] is based on two assumptions: (a) the impacts occur when velocity of the primary system is maximal; (b) the velocities of the colliding masses are opposite during the impacts. The analysis of the dynamics of the system considered in this manuscript, reveals that in order to find the optimal height, the mentioned conditions have to be modified and enriched with two additional requirements which are described in details in the following sections.

The additional novelty of the current paper is the approach adopted for the ATPID modelling. The proposed model is based on the extension of Hertzian contact theory to the nonlinear viscoelastic contact force model and reflects the physical phenomena of grain–container collisions, which are crucial for damper operation. The proposed model allows to reveal the operating principle of the ATPID damper and to conduct sensitivity analysis of the vibration damping process with respect to the height of the container, the variable mass of the granular material and the amplitude of the excitation. The obtained results are further used to optimize the ATPID parameters for the applied type of external excitation in order to maximize the effectiveness of vibration damping. Eventually, the conducted holistic analyses allow to propose a real-time control strategy providing adaptation of the ATPID damper to changing the amplitude of a kinematic excitation. Experimental verification of the proposed control strategy proves its high effectiveness.

2. ATPID construction and modelling

2.1. ATPID construction

In the classical design the, PID absorber consists of a container and granular material enclosed inside. As a result of applied external excitation the particles move and collide against the walls of the container. These collisions influence the motion of the mechanical system to which the Particle Impact Damper is attached and cause a decrease of its vibration amplitudes. One of the most important parameter influencing the damping ability is a damper height. Therefore, the main goal was to design a damper construction with the possibility of control of the container ceiling (Fig. 1).

A single grain system is often used for describing PID operations and such an approach is also implemented in the proposed concept. The considered ATPID absorber consists of the cylindrical container (1) containing a single grain (2) made of the Polylactide (PLA), moveable plate (3) joined by screw connections (4) and clutch (5) with an electric engine (6). Rotation of the engine shaft (7) is transformed into the linear movement of the plate in a vertical direction. A simple electromechanical system allows control of the electric motor, in particular the direction of movement and the velocity of the upper damper wall. This approach allows for dynamic tuning of the distance between a lower wall (floor) and an upper wall (ceiling) of the damper, and changing the volume of the chamber occupied by a particle in real-time. The 3D model and prototype of the ATPID damper are presented in Figs. 1(a) and 1(b), respectively.

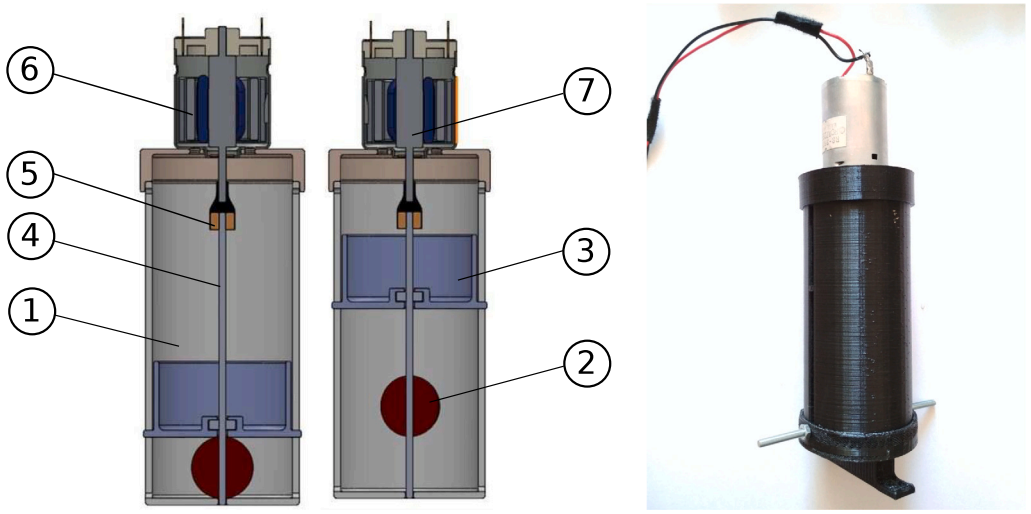

(a) ATPID 3D model (b) ATPID prototype

Fig. 1. ATPID model and prototype.

2.2. General problem of the contact modelling

The crucial phenomena in PID modelling are the impacts between the particle and container walls and the corresponding process of energy dissipation. In the previous studies of the modelling stage, soft and hard contact models were applied. The first group of them is based on a definition of the contact force in terms of grain overlap and overlap rate. These two parameters allow to describe the most possible contact schemes and include the effects of an elastic repulsion and viscous dissipation. In such an approach linear and nonlinear definitions of the contact force are based mainly on Hertz theory. On the other hand, described in the previous section the hard contact model can also be used. In our research we have decided to apply a soft contact model which describes physical effects occurring during collisions of grain more precisely, accepting a larger computational cost.

The phenomenon of the interaction of two bodies requires a general mathematical description of the contact mechanics. Several fundamental laws describing an elastic contact have been proposed by Hertz. [43]. In particular, Hertzian contact theory allows to determine the interaction between a flat surface of the specimen and a spherical indenter, where a radius of contact circle a takes the form:

$$a^3 = \frac{3RF_c}{4E_{eff}} \tag{1}$$

where R is the indenter radius, F_c is the indenter force and E_{eff} is the effective Young's modulus of the specimen and indenter defined as:

$$\frac{1}{E_{eff}} = \frac{1-\nu_w^2}{E_w} + \frac{1-\nu_p^2}{E_p} \tag{2}$$

where E_w is the specimen Young's modulus, E_p is the indenter Young's modulus, ν_w is the specimen Poisson's ratio and ν_p is the indenter Poisson's ratio. Subscripts w and p correspond to the container wall and particle (grain), respectively. Hertz also described the overlap ξ in terms of radius of contact circle a and indenter radius R:

$$\xi = \frac{a^2}{R} \tag{3}$$

Using Eqs. (1) and (3), the overlap can be written as:

$$\xi^3 = \left(\frac{3}{4E_{eff}}\right)^2 \frac{F_c^2}{R} \tag{4}$$

The transformation of the Eq. (4) allows to define a function of the elastic contact force:

$$F_c = \frac{4}{3} E_{eff} \sqrt{R} \xi^{\frac{3}{2}} \tag{5}$$

In most cases, two colliding bodies exhibit viscoelastic properties which require simultaneous consideration in the modelling process. In such a case, the general solution is described by an extension of the Hertz elastic contact force by an additional viscous part:

$$F_c = \frac{4}{3} E_{eff} \sqrt{R} \xi^{\frac{3}{2}} + \alpha \dot{\xi} \tag{6}$$

where α is a damping factor and $\dot{\xi}$ is an overlap rate. According to the classical theory of the mechanical system oscillation, the damping factor α can be expressed as a function of the system damping ratio β, mass m and stiffness k.

$$\alpha = 2\beta\sqrt{km} \tag{7}$$

Following the approach proposed by Tsuji [21], the stiffness k can be expressed as:

$$k = \frac{4}{3} E_{eff} \sqrt{R} \xi^{\frac{1}{2}} \tag{8}$$

Using Eqs. (6)–(8), a viscoelastic form of the contact force can be found:

$$F_c = \frac{4}{3} E_{eff} \sqrt{R} \xi^{\frac{3}{2}} + 2\beta \sqrt{\frac{4}{3} E_{eff} \sqrt{R} \xi^{\frac{1}{2}} m} \dot{\xi} \tag{9}$$

By introducing reduced parameters of effective stiffness k_{eff} and damping c_{eff}:

$$k_{eff} = \frac{4}{3} E_{eff} \sqrt{R} \tag{10}$$

$$c_{eff} = 2\beta\sqrt{k_{eff} m} \tag{11}$$

the viscoelastic contact force can be eventually defined by the formula:

$$F_c = k_{eff} \xi^{\frac{3}{2}} + c_{eff} \dot{\xi} \xi^{\frac{1}{4}} \tag{12}$$

2.3. ATPID modelling

In the proposed approach the ATPID damper is described as a system consisting of a container and a single particle (grain), see Fig. 2. The main assumption of the mathematical model is that the direction of grain movement is the same as the direction of the absorber motion. This means that the movement of a particle in the direction perpendicular to the direction of absorber motion (and corresponding contact forces) is omitted in the model. As it was previously mentioned the only type of contact that occurs in the ATPID damper is the grain–container contact. The result is the appearance of two contact forces: grain–floor F_{c_1} and grain–ceiling F_{c_2}.

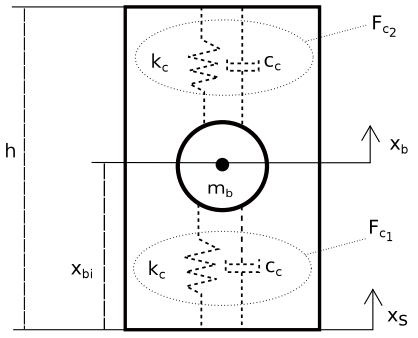

Fig. 2. Mathematical basic model of the ATPID damper.

The contact forces are described by nonlinear contact model (Eq. (12)). In the proposed approach, the forces F_{c_1}, F_{c_2} are the functions of grain overlaps (ξ_{c_1}, ξ_{c_2}) and overlaps rates ($\dot{\xi}_{c_1}$, $\dot{\xi}_{c_2}$) and they are defined as follows:

$$F_{c_1} = k_c \xi_{c_1}^{3/2} + c_c \dot{\xi}_{c_1} \xi_{c_1}^{1/4} \tag{13}$$

$$F_{c_2} = k_c \xi_{c_2}^{3/2} + c_c \dot{\xi}_{c_2} \xi_{c_2}^{1/4} \tag{14}$$

where: ξ_{c_1}, $\dot{\xi}_{c_1}$ — overlap and overlap rate of the grain during the floor impact, ξ_{c_2}, $\dot{\xi}_{c_2}$ — overlap and overlap rate of the grain during the ceiling impact, k_c — reduced effective stiffness, c_c — reduced effective damping. The grain–container reduced effective stiffness is calculated using geometrical parameters and elastic material properties of grain and container walls, according to Eq. (10):

$$k_c = \frac{4}{3} E_{eff} \sqrt{r} \tag{15}$$

where r is the grain radius and effective Young's modulus has a form given by Eq. (2). The reduced damping parameter c_c is determined according to Eq. (11), assuming a critical damping condition ($\beta = 1$) and mass of the grain m_g:

$$c_c = 2\sqrt{k_c m_g} \tag{16}$$

Analysis of Eqs. (13) and (14), for specific values of stiffness and damping parameters, shows that defined contact forces can take negative values. In order to eliminate the above non-physical effect in further computations, we will consider only positive values of contact forces by limiting the overlap value during rebound of the grain from each container wall.

Assuming the controllable container height h, its velocity $\dot{h}$, the initial position of grain x_{g_i}, its radius r, displacement of the container x_s, displacement of grain x_g, velocity of the container $\dot{x}_s$ and velocity of the grain $\dot{x}_g$ the overlaps and overlaps rates can be described by the following equations:

$$\xi_{c_1} = \begin{cases} -x_{g_i} + r + x_s - x_g & \text{if } -x_{g_i} + r + x_s - x_g > 0 \\ 0 & \text{if } -x_{g_i} + r + x_s - x_g \le 0 \end{cases} \tag{17}$$

$$\dot{\xi}_{c_1} = (\dot{x}_s - \dot{x}_g) sgn(\xi_{c_1}) \tag{18}$$

$$\xi_{c_2} = \begin{cases} x_{g_i} + r + x_g - x_s - h & \text{if } x_{g_i} + r + x_g - x_s - h > 0 \\ 0 & \text{if } x_{g_i} + r + x_g - x_s - h \le 0 \end{cases} \tag{19}$$

$$\dot{\xi}_{c_2} = (\dot{x}_g - \dot{x}_s - \dot{h}) sgn(\xi_{c_2}) \tag{20}$$

Taking into account the definitions of the overlaps Eq. (17), Eq. (19) and overlaps rates Eq. (18), Eq. (20) the definitions of both contact forces for the case of positive overlaps take the form:

$$F_{c_1} = k_c(-x_{g_i} + r + x_s - x_g)^{3/2} + c_c(\dot{x}_s - \dot{x}_g)(-x_{g_i} + r + x_s - x_g)^{1/4} \quad \text{if } \xi_{c_1} > 0 \tag{21}$$

$$F_{c_2} = k_c(x_{g_i} + r - h + x_g - x_s)^{3/2} + c_c(\dot{x}_g - \dot{x}_s - \dot{h})(x_{g_i} + r - h + x_g - x_s)^{1/4} \quad \text{if } \xi_{c_2} > 0 \tag{22}$$

The novel and one of the most interesting components of the model is a controllable ATPID height h. Its influence on the damper response is revealed by Eq. (22) which shows a strong nonlinear dependence between time-dependent damper height, its time-derivative and upper contact force F_{c_2}. Let us note that the ATPID height influences particle velocity after the collision with the damper ceiling and thus it indirectly affects the value of the lower contact force F_{c_1}.

The function of height of damper container is defined using a minimal position of the ceiling h_{min} which indicates the case when the grain is blocked, the controllable range of ceiling movement Δh and dimensionless control function $0 < \psi < 1$ describing characteristics of the changes:

$$h = h_{min} + \Delta h \psi \tag{23}$$

The proposed control function ψ can take an arbitrary form which can describe a real movement of the damper height controlling element. Herein, we use a linear control function with two different tuning times. The application of the linear change of the damper height is also caused by practical aspects of system implementation. The proposed control function directly depends on the method of changing the position of the container ceiling during experimental tests. These depend on the used electric motor. The motor was powered by a constant current, which caused a linear change of the position of the damper ceiling.

$$\psi = \begin{cases} 0 & \text{if } t < t_1 \\ \frac{t - t_1}{\Delta t_{12}} & \text{if } t_1 < t < t_2 \\ 1 & \text{if } t > t_2 \end{cases} \tag{24}$$

where: t — control time, t_1 — activation start time, t_2 — saturation start time, $\Delta t_{12} = t_2 - t_1$ — activation period.

Eventually, the complete model of the ATPID damper contains definition of generated force expressed with the use of contact forces defined by Eqs. (21) and (22) and equation of motion of the grain:

$$F_{ATPID} = -F_{c_1}(x_s, x_g, \dot{x}_s, \dot{x}_g) + F_{c_2}(x_s, x_g, \dot{x}_s, \dot{x}_g, h, \dot{h}) \tag{25}$$

$$m_g \ddot{x}_g - F_{c_1}(x_s, x_g, \dot{x}_s, \dot{x}_g) + F_{c_2}(x_s, x_g, \dot{x}_s, \dot{x}_g, h, \dot{h}) + Q_g = 0 \tag{26}$$

where Q_g is the grain gravity force. Solution of the equation of grain motion is necessary to obtain the displacement of the grain x_g and contact forces resulting from applied kinematic excitation given by displacement x_s. The model composed of Eqs. (25) and (26) allows to determine the force generated by the ATPID absorber under an arbitrary kinematic excitation.

3. Experimental and numerical study

3.1. Test stand and numerical scheme

The designed laboratory testing stand allows to investigate the effectiveness of the ATPID absorber in damping of vibrations of the cantilever beam (Figs. 3 and 4). The test stand consists of an electric motor with an eccentric disc (1), a system that converts rotary motion into a linear one (2), a beam (3), a designed ATPID damper (4), a data transmission system (5), a control system (6), two inverters (7), a power supply (8) and a data analysis system (9). To perform the described experimental research, the authors applied: excitation amplitude ± 10 [mm], maximum excitation frequency 3.5 [Hz]. The quantity measured during the experiment was the displacement of the beam free end. For this purpose, a laser sensor ZX1-LD300A81 Omron and measuring card Labjack T7-pro were used.

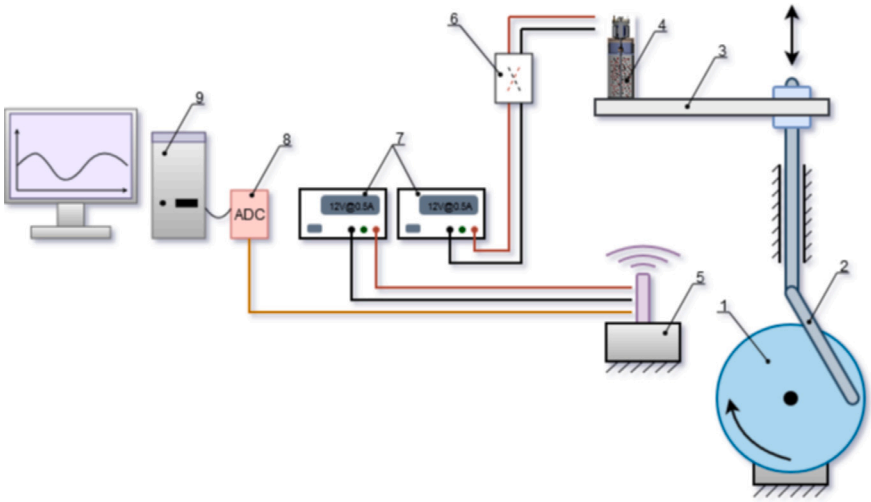

Fig. 3. Scheme of the experimental test stand.

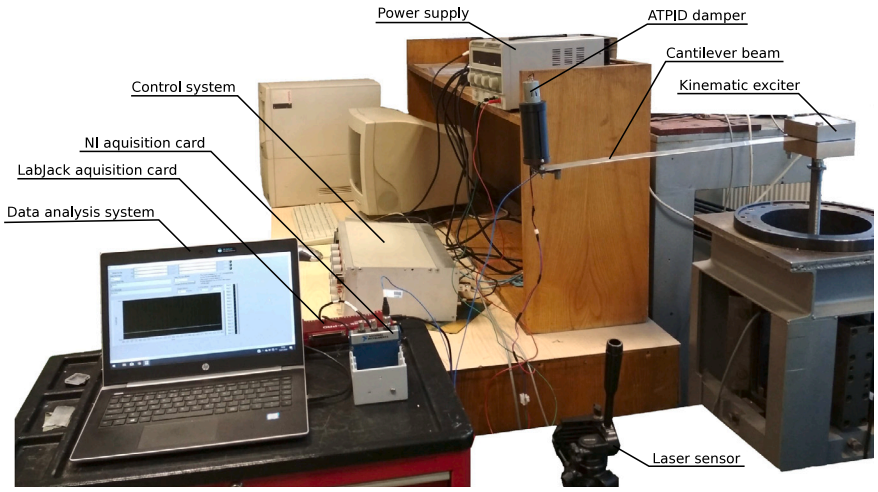

Fig. 4. Experimental test stand.

The scheme of the tested mechanical system is presented in Fig. 5. The corresponding mathematical model of the system is developed using the damper model derived in Section 2. The governing equations and initial conditions of the proposed model are given by Eqs. (27)–(29).

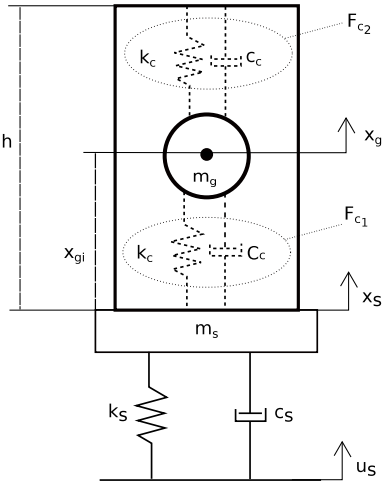

Fig. 5. Scheme of the ATPID construction.

$$m_s\ddot{x}_s + F_{ext} - F_{ATPID}(x_s, x_g, \dot{x}_s, \dot{x}_g, h, \dot{h}) + Q_s = 0 \tag{27}$$

$$m_g\ddot{x}_g + F_{ATPID}(x_s, x_g, \dot{x}_s, \dot{x}_g, h, \dot{h}) + Q_g = 0 \tag{28}$$

$$F_{ext} = k_s[x_s - u_s] + c_s[\dot{x}_s - \dot{u}_s] \tag{29}$$

$$\dot{x}_s(t=0) = 0, \quad x_s(t=0) = -\frac{(m_s + m_g)g}{k_s} \tag{30}$$

$$\dot{x}_g(t=0) = 0, \quad x_g(t=0) = -\frac{(m_s + m_g)g}{k_s} + x_{g_i} \tag{31}$$

The model contains the beam (primary system) parameters: m_s — reduced mass, k_s — reduced stiffness, c_s — reduced damping, $\ddot{x}_s$ — beam acceleration, $\dot{x}_s$ — beam velocity, x_s — beam displacement, $Q_s = m_s g$ — beam gravity force; the grain parameters: m_g — grain mass, $\ddot{x}_g$ — grain acceleration, $\dot{x}_g$ — grain velocity, x_g — grain displacement, $x_{g_i} = r$ — initial position of the grain in the container, $Q_g = m_g g$ — grain gravity force; g — gravity; and excitation parameters: $\dot{u}_s$ — support velocity, u_s — support displacement. Moreover, F_{ATPID} is a total force generated by the ATPID damper defined by Eq. (25).

The introduced initial conditions allow to obtain a static equilibrium of the system at the initial stage of the simulations. In the further part of the analysis, the displacements of the beam, container and grain are shifted by $x_s(t=0)$ to get the beam's oscillations around the initial equilibrium position.

The applied kinematic excitation is defined by function describing the motion of the structure support, given by the equation:

$$u_s = A\sin(2\pi f t) \tag{32}$$

where the resonance frequency f depends on mass m_s and m_g as follows:

$$f = \frac{\sqrt{k_s}}{2\pi\sqrt{m_s + m_g}} \tag{33}$$

and amplitude of excitation $A = 10$ [mm].

The simulation of the dynamic response of the system subjected to above defined excitation includes phenomena such as multiple grain–walls collisions described the nonlinear contact model and characterized by very short duration time. Therefore, the equations of motion require numerical solutions using appropriate time-integration methods and a detailed analysis of their accuracy. In practice, several different numerical methods were used to conduct numerical simulation, including Fehlberg fourth–fifth order Runge–Kutta method (RKF45), Cash–Karp fourth–fifth order Runge–Kutta method (CK45), Implicit Rosenbrock third–fourth order Runge–Kutta method (Rosenbrock) and Livermore Solver for Ordinary Differential Equations (LSODE). A series of the calculations performed in the MAPLE software revealed that the results for various methods are similar when an absolute error tolerance and a relative error tolerance are very small and close to 10^{-10}.

In the following parts of the paper, the attention is focused on the influence of various grain and container parameters on the response of the system, including generated contact forces, system kinematics and resulting efficiency of vibrations damping. At the beginning of each simulation, such parameters are presented in the form of tables.

3.2. Comparison of experiments and numerical simulations

In order to validate the proposed mathematical model given by Eqs. (27)–(31) the results of basic experiments and numerical simulations assuming reduced parameters of the system were thoroughly compared against each other. The experimental object was a cantilever beam with mass $m_b = 0.36$ [kg], which was reduced to the 1-DOF system in the numerical simulations. Reduced stiffness K_s corresponding to the first mode of vibrations was calculated in a standard manner. Natural frequencies of the system were found by spectrum analysis of experimental free vibrations of the tested object. The reduced mass was determined as $m_s = 0.905 m_b$ in order to obtain the mathematical model with an exact value of the first natural frequency (3.02 [Hz]) for the calculated reduced stiffness. Reduced damping C_s was identified to obtain similar numerical and experimental amplitudes of the free vibrations.

The next stage of modelling was finding the reduced mass of the grain m_g. In the experimental study, the mass of the grain was assumed as 10% and 5% of the total mass of the tested system and the first natural frequency were 2.862 [Hz] and 2.944 [Hz], respectively. In the numerical case, a similar approach was implemented and the reduced mass of the grain was assumed as 10% and 5% of the total mass of the reduced system, which resulted in similar values of the first system eigenfrequencies equal to 2.868 [Hz] and 2.947 [Hz], respectively. Physical parameters of the reduced tested object (k_s, c_s, ν_w, ν_p, E_w, E_p) are either a priori known or computed based on the preliminary experiments and presented in the Table 1.

Table 1
Basic simulations parameters.

k_s	c_s	$\nu_p = \nu_w$	$E_w = E_p$
117.6 [N/m]	0.56 [Ns/m]	0.2	$2.1 \cdot 10^8$ [Pa]

The assumed control function ψ was based on the activation start time $t_1 = 6$ [s] and the activation period $\Delta t_{12} = 1$ [s]. The controllable damper height described by Eq. (23) assumed two various minimal heights: 0.01 [m] for grain mass equal to $0.05M$ (Fig. 6(a)) and 0.017 [m] for grain mass equal to $0.1M$ (Fig. 6(b)). In both cases, the maximal container height (h_{max}) was equal 0.1 [m].

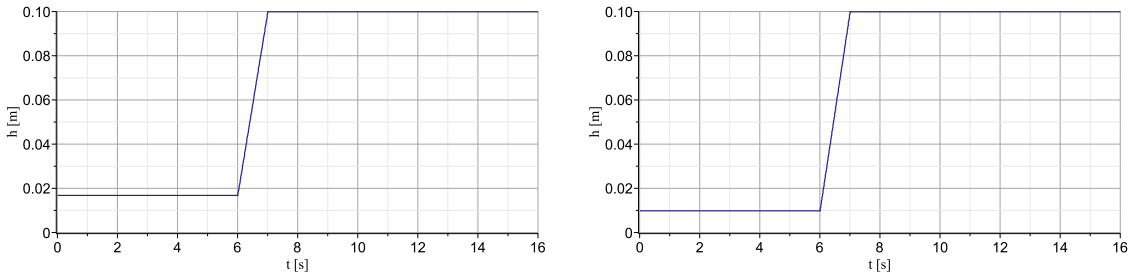

(a) $h_{min} = 0.01$, $m_g = 0.05 M_s$ (b) $h_{min} = 0.017$, $m_g = 0.1 M_s$

Fig. 6. Controllable damper heights.

All other parameters of the container and particle required for the simulation can be found in the Table 2. Results of the conducted simulations of system vibrations are presented in Figs. 7 and 8.

Table 2
Parameters used in simulations.

m_g	h_{min} [m]	h_{max} [m]	r [m]	k_c [$\frac{N}{m^{3/2}}$]	c_c [$\frac{Ns}{m^{3/4}}$]
$0.05M$	0.01	0.1	0.05	$1.031 \cdot 10^7$	841
$0.1M$	0.017	0.1	0.085	$1.344 \cdot 10^7$	1395.3

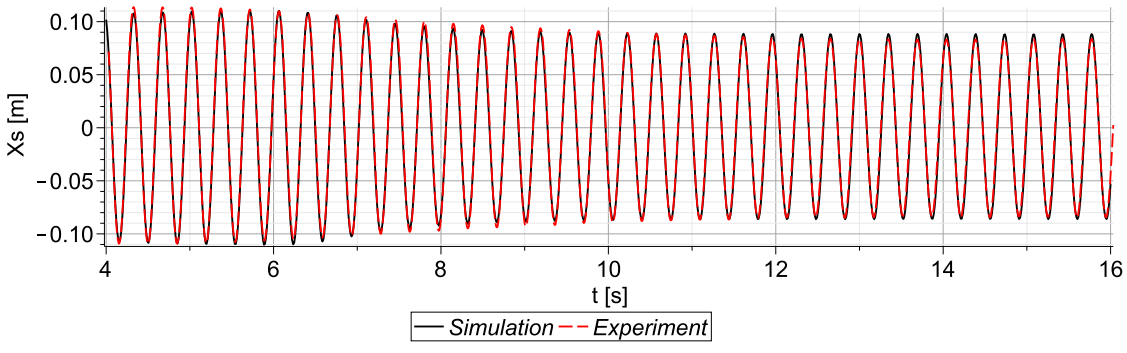

Fig. 7. Comparison of the experimental and numerical results, $m_g = 0.05M$.

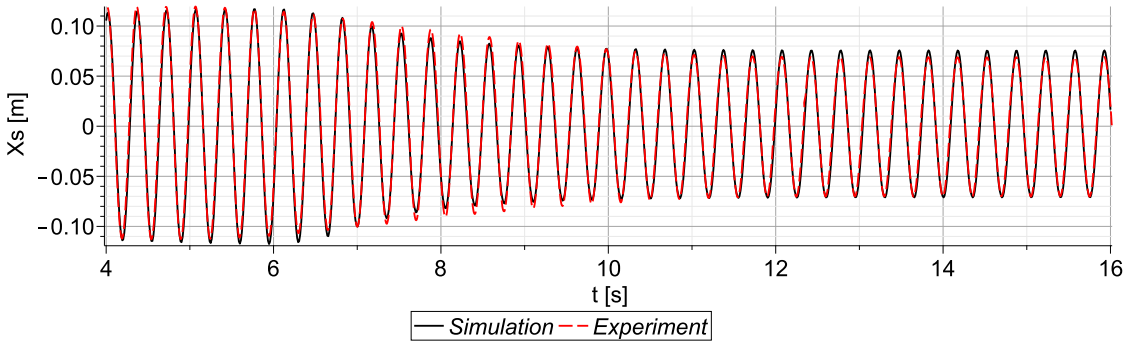

Fig. 8. Comparison of the experimental and numerical results, $m_g = 0.1M$.

Response of the beam under proposed harmonic excitation can be divided to the three main stages:

- The first stage when the grain is blocked ($h = h_{min}$) and then the vibration is resonant and stabilized in range 4 [s]$< t <$ 6 [s].
- The second stage when the controlling process was activated and the damper ceiling reached the maximum height in one second but the stabilization time of the beam vibration takes more than three seconds in both considered cases.
- The third stage when beam vibrations are damped and a steady-state can be observed in range 12 [s]$< t <$14 [s].

Presented results enable effective validation of the proposed mathematical model for two different grain mass values. In both presented cases the amplitudes of displacements obtained from the experiments and numerical simulations closely coincide. Moreover, the agreement of both results holds for various amplitudes and frequencies of the kinematic excitation. The above comparison indicates that numerical simulations based on the proposed mathematical model can be efficiently used to investigate an operation of the ATPID damper.

For each simulation X_{Sim} and experimental X_{Exp} result, the Root Mean Square Errors (RMSE) of the beam displacements corresponding to intervals of the transient (6 [s] $< t <$ 10 [s]) and damped ($t >$ 10 [s]) vibrations were calculated according to the formula:

$$RMSE = RMS\left(\frac{X_{Exp} - X_{Sim}}{X_{Exp}}\right) \tag{34}$$

The above parameter was calculated for 5 different masses of grain (1%, 2.5%, 5%, 10%, 20%) and for various excitation frequencies (0.9, 0.95, 1, 1.05, 1.1 of resonance frequency value). The values of the RMSE of beam displacements for a range of transient vibrations are presented in the Table 3 and for a range of steady-state damped vibrations in the Table 4. The proposed approach allowed to present the errors between the experiment and the simulation in the resonance range and in its vicinity when the grain collides against both container walls.

Table 3
RMSE comparison of vibrations in transient range.

	$0.9f_{res}$	$0.95f_{res}$	f_{res}	$1.05f_{res}$	$1.1f_{res}$
$0.01M$	0.016	0.079	0.059	0.062	0.019
$0.025M$	0.018	0.09	0.067	0.7	0.025
$0.05M$	0.019	0.1	0.075	0.079	0.032
$0.1M$	0.022	0.115	0.084	0.089	0.035
$0.2M$	0.027	0.129	0.094	0.101	0.039

Table 4
RMSE comparison of vibrations in steady-state range.

	$0.9f_{res}$	$0.95f_{res}$	f_{res}	$1.05f_{res}$	$1.1f_{res}$
$0.01M$	0.019	0.087	0.075	0.08	0.023
$0.025M$	0.019	0.079	0.07	0.073	0.02
$0.05M$	0.018	0.073	0.064	0.067	0.017
$0.1M$	0.015	0.067	0.058	0.062	0.015
$0.2M$	0.012	0.061	0.053	0.057	0.014

The results presented in the Tables 3 and 4 show that the differences of system response for resonance excitations are acceptable in both assumed ranges: from 0.059 to 0.094 for a transient vibrations and from 0.053 to 0.075 for steady-state vibrations. The increase of the RMSE coefficient for the ranges around resonance is visible, however, their values are also small (maximum 0.129 for a transient range, and maximum 0.087 for a steady-state range). The obtained results prove that the proposed mathematical model can be successfully used for further numerical analyses.

4. Principles of the ATPID operation

The analysis of the governing equations of the proposed system (Eqs. (27) and (28)) shows that the operation of the ATPID damper is complicated and requires further investigation. A better understanding of the analysed dynamic process can be gained by introducing the relation between contact forces determined from the equation of grain motion (Eq. (28)) into the equation of system motion (Eq. (27)). The resulting equation can be written in two equivalent forms:

$$(m_s + m_g)(\ddot{x}_s + g) - m_g\left(1 - \frac{\ddot{x}_g + g}{\ddot{x}_s + g}\right)(\ddot{x}_s + g) + F_{ext} = 0 \tag{35}$$

$$(m_s + m_g)(\ddot{x}_s + g) + m_g(\ddot{x}_g - \ddot{x}_s) + F_{ext} = 0 \tag{36}$$

The first component of Eqs. (35) and (36) describes an initial state of the analysed system when the grain cannot move inside the container ($h_{max} = 2r$) and thus the total system mass is the sum of basic structure mass and grain mass ($M = m_s + m_g$). The second component is identical in both equations but can be interpreted in two different manners as two distinct principles of ATPID operation. In Eq. (35) the first term of the second component describes the Mass Modification Effect (MME), which represents a change of system mass ΔM resulting from the presence of the moving grain. In turn, in Eq. (36) the second component describes the Pseudo-Inertial Force Effect ($PIFE$), which represents additional force F_{iner} resulting from grain movement. The PIFE effect is introduced in order to reveal the mathematical relation and mathematical similarity between the ATPID damper and currently popular mechanical systems called inverters, which utilize inertial forces depending on the relative acceleration of the system components [44,45]. Both above operating principles describe a transition between three possible specific states of the system.

The first state occurs when the accelerations of the container and the grain are approximately equal $\ddot{x}_g \approx \ddot{x}_s$, which corresponds to the mentioned above initial state of closed damper or to the situation when grain can move ($h_{max} > 2r$) and is pushed by one of the container walls. In such cases, both the terms indicating mass modification in Eq. (35) and the term indicating inertial force in Eq. (36) are equal to zero. Consequently, the two degrees of freedom (2–DOF) system can be replaced by 1–DOF system of total mass $M = m_s + m_g$, described by the equation:

$$(m_s + m_g)(\ddot{x}_s + g) + F_{ext} = 0 \tag{37}$$

In turn, the second state is when the grain is free-flying without any collisions with container walls ($\ddot{x}_g = -g$). Then, the terms indicating mass modification in Eq. (35) and inertial force in Eq. (36) are equal:

$$\Delta M = -m_g, \tag{38}$$

$$F_{iner} = -m_g(\ddot{x}_s + g) \tag{39}$$

In such a case, mass modification term indicates a reduction of total system mass by grain mass, while pseudo-inertial force term has untypical form including grain mass and system acceleration. Consequently, the equivalent 1-DOF system consists only of beam mass ($M = m_s$) and it is described by the equation:

$$m_s(\ddot{x}_s + g) + F_{ext} = 0 \tag{40}$$

Finally, the third state indicates the situation when the accelerations of the grain and container are significantly different $\ddot{x}_g \neq \ddot{x}_s$, which corresponds to the phenomenon of the occurrence of a short impact with the rebound of the grain from the container wall. Then, the terms indicating mass modification in Eq. (35) and inertial force in Eq. (36) take general forms:

$$\Delta M = -m_g\left(1 - \frac{\ddot{x}_g + g}{\ddot{x}_s + g}\right) \tag{41}$$

$$F_{iner} = m_g(\ddot{x}_g - \ddot{x}_s) \tag{42}$$

In such a case, the mass modification term describes a short and rapid change of the system mass, while the pseudo-inertial force term indicates the short and rapid change of additional force. Both these terms depend on the mass of the grain as well as accelerations of grain and mass. Moreover, they can assume both positive and negative values depending on the scenario of grain–wall collision. The model of the equivalent 1-DOF system contains full definitions of mass modification terms and pseudo-inertial terms, and it is defined by two equivalent equations Eqs. (35) and (36).

The MME effect can be revealed by considering free vibrations of the system with ATPID damper (Fig. 9) and analysing their spectrum (Fig. 10). All parameters used in the further simulations are as follows: $m_s = 0.905m_b$ [kg], $m_g = 0.1M$, $k_s = 427.6$ [$\frac{\mathrm{N}}{\mathrm{m}}$], $c_s = 0.56$ [$\frac{\mathrm{Ns}}{\mathrm{m}}$], $\nu_p = \nu_w = 0.2$, $k_c = 1.334 \cdot 10^7$ [$\frac{\mathrm{N}}{\mathrm{m}^{3/2}}$], $c_c = 1395.3$ [$\frac{\mathrm{Ns}}{\mathrm{m}^{5/4}}$], $E_p = E_w = 2 \cdot 10^8$ [Pa].

The presented spectrum change can be considered as an example of the MME. The natural frequency of vibrations the whole system for a low container height ($h = 0.017$ [m]) is $f = 5.49$ [Hz], which corresponds to the mass of the system consisting of a beam, ATPID compartment and grain. In turn, the natural frequency of vibrations for a larger container height ($h = 0.4$ [m] or $h = 0.6$ [m]) equals $f = 5.77$ [Hz], which refers system composed of a beam and the damper container without the grain. For other cases of the container height, the eigenfrequencies are between above extreme values, which means that the dynamic characteristics of the system are changeable and generally depend on the damper ceiling position. Although the natural frequencies of the system for two cases $h_{max} = 0.4$ [m] and $h_{max} = 0.6$ [m] are very similar ($f = 5.77$ [Hz]), the amplitude of the vibrations for a larger container height is significantly higher.

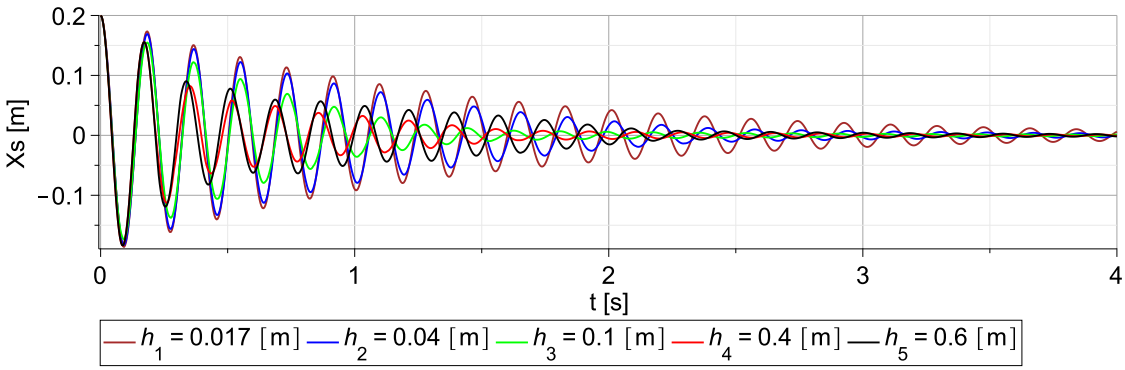

Fig. 9. Free vibrations for various ATPID heights.

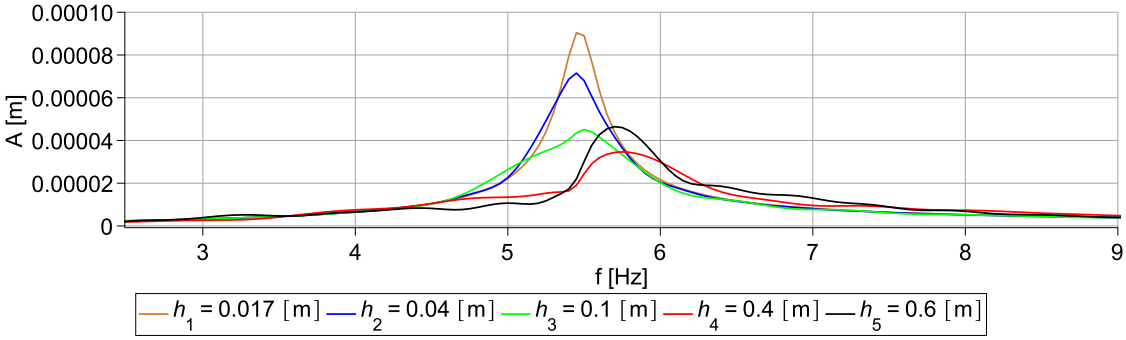

Fig. 10. Spectrum of free vibrations.

It should be noticed that the effective mass of the system for two cases of the container heights $h_{max} = 0.4$ [m] and $h_{max} = 0.6$ [m] is similar what is observed in the eigenfrequencies ($f = 5.77$ [Hz]) but the amplitude of the vibrations for a higher container height is significantly larger. In order to reveal the reason of the worse damping of the system for larger container height, the complete kinematics of the system (ATPID floor, ceiling and grain displacements) for two mentioned container heights were presented in Fig. 11.

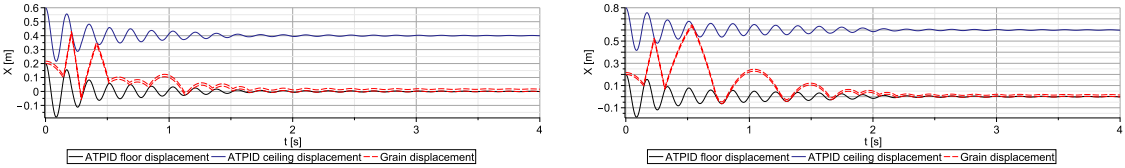

(a) $h = 0.4$ [m]. (b) $h = 0.6$ [m].

Fig. 11. Damper (floor and ceiling) and grain movement for various container heights.

In the case $h_{max} = 0.4$ [m], the regular collisions of the grain with container floor and ceiling are observed during the initial two cycles of vibrations. In contrast, in the case $h_{max} = 0.6$ [m] the grain impacts occur irregularly in random cycles of the process. Better damping of the system is observed in the first case because collisions occur during a longer period of vibrations. Moreover, worse damping capabilities in the second case are described by the Mass Modification Effect and the Pseudo-Inertial Force Effect (second components of Eqs. (35) and (36)), which become unpredictable and occur in random states of beam response.

The principle of ATPID operation can be explained by analysing the change of system energy during the analysed process of free vibrations. The energy balance of the system can be obtained by integration of the equation of beam motion over its displacement:

$$\int_{\Delta x_s} m_s \ddot{x}_s \mathrm{d}x_s + \int_{\Delta x_s} F^s_{ext} \mathrm{d}x_s + \int_{\Delta x_s} (F_{c_1} - F_{c_2}) \mathrm{d}x_s + \int_{\Delta x_s} Q_s \mathrm{d}x_s = 0 \tag{43}$$

By identifying the subsequent terms of Eq. (43) as the change of kinetic energy ΔE^s_k, change of elastic energy ΔE^s_{el}, viscous dissipation W^s_d and change of potential energy ΔE^s_p the equation of the energy balance can be written in a form:

$$\Delta E^s_k + \Delta E^s_{el} + W^s_d + \int_{\Delta x_s} (F_{c_1} - F_{c_2}) \mathrm{d}x_s + \Delta E^s_p = 0 \tag{44}$$

The total energy of the beam E^s_{tot} can be defined as a sum of kinetic E^s_k, elastic E^s_{el} and potential energy E^s_p, and according to Eq. (44), its change ΔE^s_{tot} is caused by work done by contact forces generated in ATPID damper and viscous dissipation W^s_d:

$$\Delta E^s_{tot} = -\int_{\Delta x_s} (F_{c_1} - F_{c_2}) \mathrm{d}x_s - W^s_d \tag{45}$$

Since viscous dissipation is uncontrollable process, the change of total beam energy and the effectiveness of the vibrations damping process is strongly influenced by work done by contact forces generated in the ATPID damper. Thus, the following numerical examples will be focused on the analysis of the changes of the integral quantity $W^s_{F_c}$ defining work of contact forces:

$$W^s_{F_c} = -\int_{\Delta x_s} (F_{c_1} - F_{c_2}) \mathrm{d}x_s = \int_{\Delta x_s} F_{ATPID} \mathrm{d}x_s \tag{46}$$

which has to be positive and possibly large in order to cause the decrease of total beam energy and efficient process of vibrations damping.

The plots presented in Fig. 12 reveal the change of work done by forces generated by ATPID damper $W^s_{F_c}$ during the first impact of the grain against the lower container wall. The work is calculated between the initial time instant of contact and time instant of the permanent detachment of both objects.

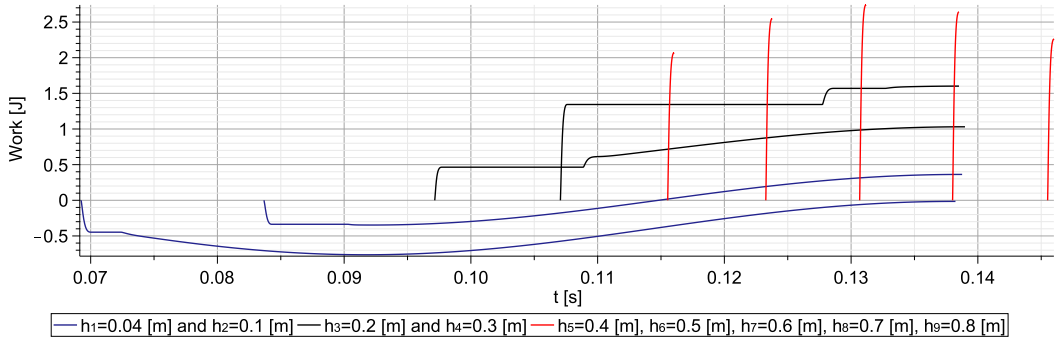

Fig. 12. Change of work done by contact forces during the first impact of grain and container wall during the process of free vibrations for various container heights.

The first group of cases (navy lines) corresponds to very low damper's heights (h_{max} = 0.04 [m] and h_{max} = 0.1 [m], which result in impact of the grain during downward movement of the container when directions of objects' motion are the same. In such a situation, the peak of contact force is followed by a short grain rebound and the phase when the grain is pushed by the lower container wall. Consequently, the work done by contact force on container displacement is negative at the beginning of impact but it gradually raises during the second stage when the beam pushes the grain upwards. As a result, at the final time instant of the process, the total work done by contact force is close to zero in the first case and assumes a small positive value in the second one.

The second group of cases (black lines) refers to larger damper's heights (h_{max} = 0.2 [m] and h_{max} = 0.3 [m]), which result in impact of the grain during upward movement of the container when directions of objects' motion are opposite. In the first case, a large rebound of the grain is followed by the second impact and the phase when the grain is pushed by the container wall. In both these processes the work done by contact forces increases. In turn, in the second case, the second impact is also followed by grain rebound and only a short pushing phase is observed at the end of the process. Consequently, the increase of work occurs mostly during the first and partially during the second impact. As a result, in both situations the work done by contact forces is substantial.

Finally, in the third group of cases the damper's heights are the largest (h_{max} = 0.4 [m], h_{max} = 0.5 [m], h_{max} = 0.6 [m], h_{max} = 0.7 [m], h_{max} = 0.8 [m]), which causes that impact occurs when container moves upwards and its velocity is relatively large. In this situation, the grain impact is followed by a permanent rebound of the grain without further contact with the lower container wall in the analysed cycle of vibrations. In all considered cases, an increase of work done by contact forces occurs during a short period of contact between the colliding bodies. The change of work becomes larger as the pre-impact velocity of the container increases and it achieves maximal value when the collision occurs in the vicinity of the equilibrium state. In the following cases, the velocity of the container wall before impact is smaller and the change of performed work diminishes.

The above analysis proves that regardless of the collision scheme, characterized by beam movement direction and its velocity, the work done by contact forces is either close to zero or assumes a positive value after each impact. Further collisions of the grain and damper's walls occur for various combinations of grain and damper movement directions and velocities but three above collision schemes are followed. Thus, the application of the ATPID damper always provides a decrease of system energy and an effective process of vibrations damping.

In order to extend the analysis of the kinematic results presented in Fig. 9, the total beam energy E^s_{tot} for each case was computed and shown in Fig. 13. The presented plots allow to analyse more precisely the longer period of the process of vibrations damping for various damper heights. In all cases, a different time of vibration stabilization is observed. In most cases, the collision between grain and container walls occurs in the situation when the direction of the grain movement is opposite to the direction of the beam movement. In such impacts, the work done by contact forces is positive and causes a decrease of total beam energy, which directly

results in effective damping of system vibrations. The events when the grain collides with the beam when the directions of their movement are the same cause a temporary decrease of work done by contact forces and an increase of the beam energy. However, such impacts do not have a large influence on the damping ability of the system.

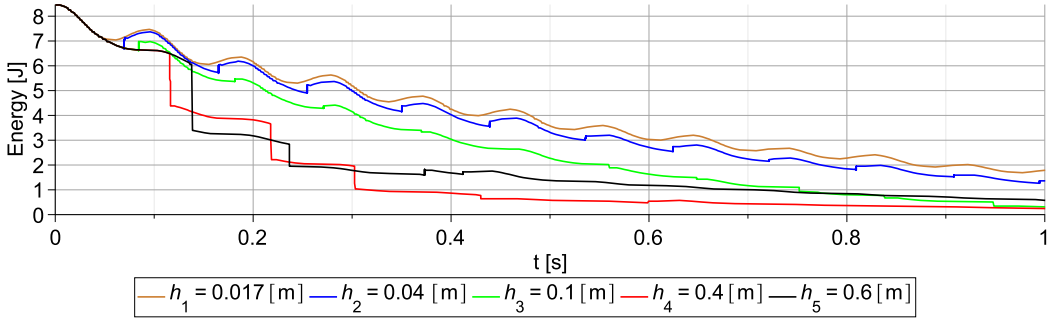

Fig. 13. The total energy of the beam E^{s}_{tot} for various container heights.

5. ATPID sensitivity analysis

In order to analyse the sensitivity of the proposed damper, the influence of various parameters (container height, grain mass and excitation amplitude) on the dynamic response of the cantilever beam under harmonic excitation was calculated using Eqs. (27)–(33). Displacements of the free end of the beam subjected to a resonance excitation for various container heights are presented in Fig. 14. Moreover, grain, container floor and ceiling displacements for various damper heights are presented in Fig. 15 and Fig. 16, for various grain mass in Fig. 17 and for various excitation amplitudes in Fig. 18.

5.1. Influence of the container height

As it was presented in Section 4, the damper height is one of the most important system parameters from the vibrations mitigation point of view. In order to understand the changes of the system dynamics related to modification of container ceiling position, five different maximal container heights ($h_1 \rightarrow h_5$) were assumed (Table 5) and the corresponding dynamic response of the system was calculated (Fig. 14). The remaining parameters of the functions h were constant and equal: $h_{min} = 0.017$ [m], $t_1 = 6.5$ [s], $t_2 = 9$ [s].

Table 5
Parameters used in simulations.

h_{max} [m]	h_1 =0.04	h_2 =0.08	h_3 =0.12	h_4 =0.16	h_5 =0.20

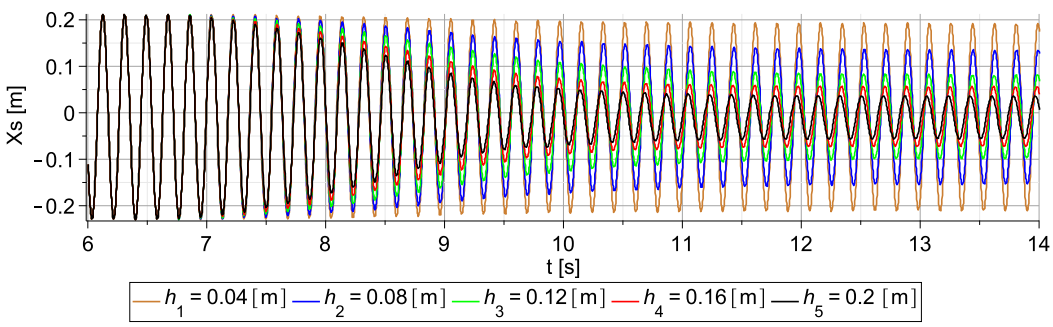

Fig. 14. Displacements of the free end of the beam for various maximal container heights — $h_1 \rightarrow h_5$.

The maximal height of the container determines a space for a movement of the grain, affects damping effectiveness and changes amplitudes of the damped system vibrations. Therefore, a correct tuning of the ceiling position is very important in the ATPID control process. The results presented in Fig. 14 show that the effectiveness of vibrations mitigation obtained for various damper heights is significantly different. The highest damping is observed in case $h_5 = 0.2$ [m] where maximal amplitude of the vibrations in the resonance range ($x_s = 0.23$[m]) is reduced by 78% and reaches 0.048 [m] in a steady-state. For other analysed maximal container heights $h_4 \rightarrow h_1$, lower damping is visible and vibration amplitudes are decreased by 71%, 57%, 32% 5%, respectively.

In order to observe the main reasons why vibrations mitigation is different for various damper heights, the extended analysis of the simulations results was conducted. The grain, container floor and ceiling displacements are presented in Fig. 15.

Presented results provide a description of the types of grain movement for various ATPID container heights. For the sake of clarity, the definitions of two impact types will be introduced. The impact with the sticking effect is the situation when after impact the grain is pushed by the container wall and thus the accelerations of the grain and the wall are similar. In turn, the short impact without sticking effect is the impact followed by immediate grain rebound, in which the accelerations of the grain and the wall are significantly different.

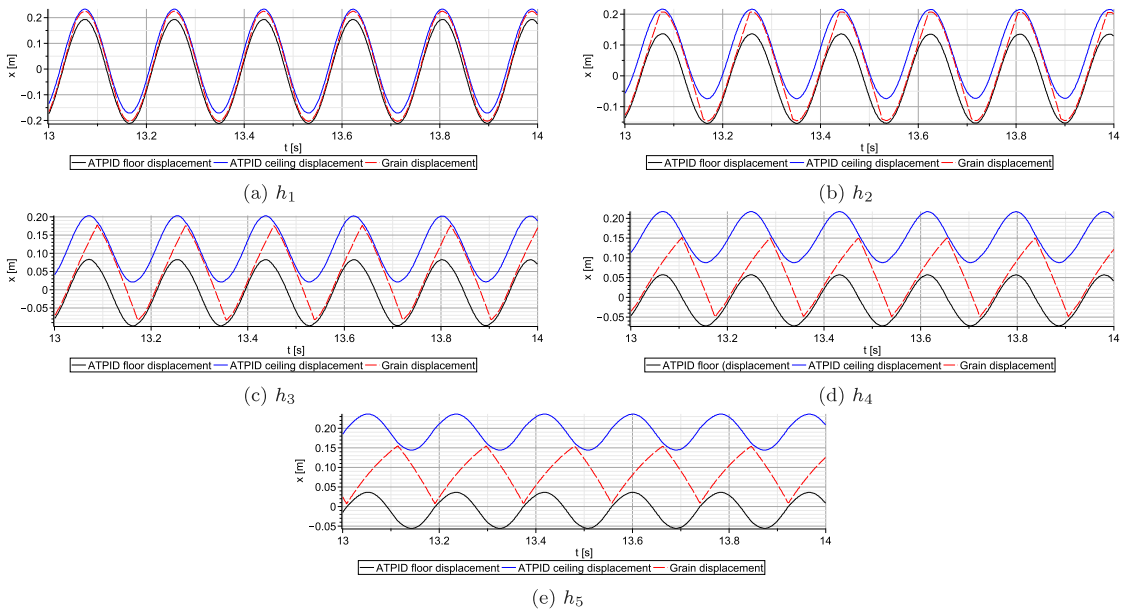

Fig. 15. Damper (floor and ceiling) and grain displacement for various container heights ($h_1 \rightarrow h_5$).

The first type of ATPID operation occurs when the damper ceiling position is relatively low ($h_1 = 0.04$ [m], $h_2 = 0.08$ [m], $h_3 = 0.12$ [m]) (Figs. 15(a)–15(c)). In such a situation, the system response can be described as a subsequent occurrence of the sticking effects between the grain and a lower or upper container wall with intermediate non-contact stages of the grain movement being much shorter than the sticking stages. As a result, the effective mass of the system and its natural frequency are similar as in the case with the closed damper. Consequently, damping abilities of the ATPID are relatively low, but they increase along with the increase of the damper height. The second type of operation arises when the damper container is significantly higher ($h_5 = 0.2$ [m]) and impacts without the sticking effect are observed in every period of vibrations (Fig. 15(e)). In this case, the mass of the entire system is substantially reduced, which was noticed in the description of Eq. (35). Consequently, the natural frequency of the system is shifted to a different range and the damping abilities of the ATPID are much larger than in the previously considered cases involving the sticking effect (Figs. 15(a)–15(c)). The third type of ATPID operation is presented in Fig. 15(d) where both mentioned effects are visible: a sticking effect between the grain and damper floor as well as an impact without a sticking effect between the grain and container ceiling.

The above analysis reveals that the ATPID damper is the most effective and the amplitudes of the steady-state vibrations are the smallest when only short grain–wall impacts (without sticking effect) occur in every period of vibrations (the second type of operation, Fig. 15(e)). The above conclusion is in agreement with a conclusion regarding ATPID effectiveness in damping of free vibrations, which was also the highest for the case of short grain impacts (cf. Fig. 12 and Fig. 13 in Section 4).

The objective of the following numerical simulations was to analyse how the particle movement will change when the ceiling position will be higher than previously considered. Two damper heights: $h_6 = 0.3$ [m] and $h_7 = 0.6$ [m] were considered. Displacements of the grain, as well as ATPID floor and ceiling, were presented in Fig. 16.

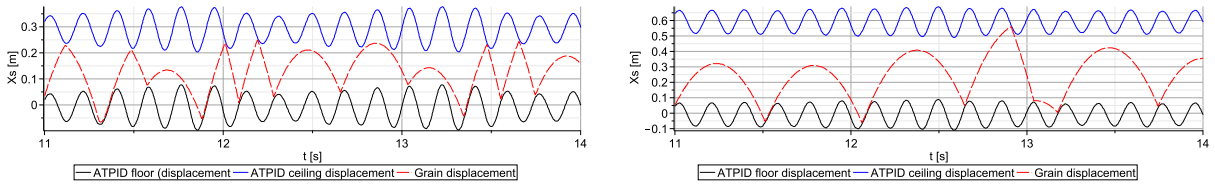

Fig. 16. Damper (floor and ceiling) and grain movement for large container heights (h_6 and h_7).

Focusing on the obtained results, two new principles of the ATPID operation can be revealed: random impacts and lack of ceiling impacts. The first type of operation (Fig. 16(a)) corresponds to the situation when the grain is in contact with both the lower and the upper wall of the container, but the collisions do not occur in every period of vibrations. The second type of operation (Fig. 16(b)) takes place when the particle cannot reach the ceiling position and impacts with the floor do not occur in every period of vibrations. Both phenomena are characterized by the unpredictable grain movement inside the container and the small efficiency of vibration damping. Therefore, they are treated as undesirable effects.

5.2. Influence of the grain mass

Another important stage of sensitivity analysis was a computation of the grain mass influence on the grain movement and the ATPID damping ability. Four different values of particle mass m_g were assumed: $m_1 = 0.05M$, $m_2 = 0.1M$, $m_3 = 0.2M$, $m_4 = 0.4M$, where $M = m_g + m_s$. For each case, the excitation frequency was assumed as a resonance frequency and it was calculated using the actual value of grain mass: $f = \sqrt{\frac{k_s}{m_g+m_s}}$. The other parameters of the analysis were: the constant height of the damper $h_{max} = 0.2$ [m] and the excitation amplitude $A = 0.01$ [m]. The displacement of the damper floor, grain and damper ceiling are presented in Fig. 17.

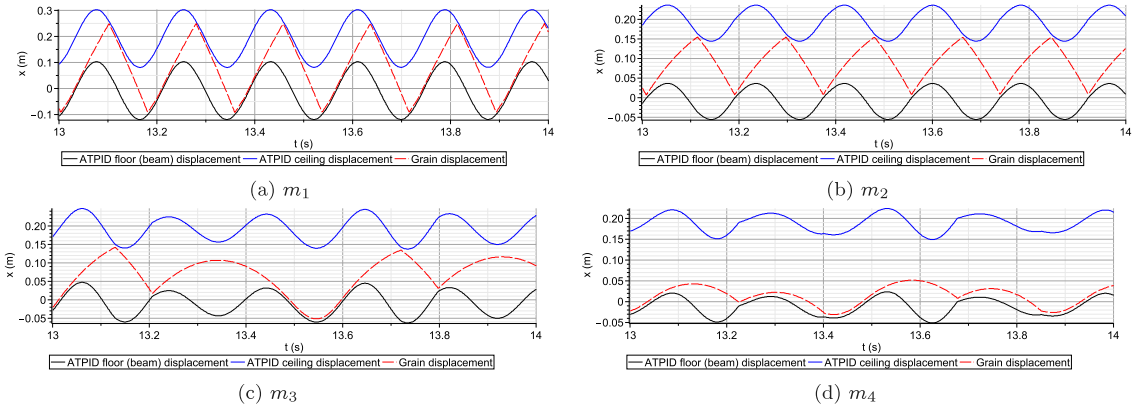

Fig. 17. Damper (floor and ceiling) and grain movement for various grain mass ($m_1 \rightarrow m_4$).

For the proposed values of the grain mass ($m_1 \rightarrow m_4$) the four previously described types of the ATPID operation can be observed. For the assumed values of the system parameters, a very low mass of the grain (m_1) causes the occurrence of the sticking effect between the grain and the damper floor or ceiling (Fig. 17(a)). A larger mass of the grain (m_2) allows to observe the most effective system damping with the non-sticking contact of the grain with the damper walls (Fig. 17(b)). Further particle mass increase reveals the undesirable effect of random collisions (Fig. 17(c)), while even larger mass causes the situation when the grain–ceiling impacts do not occur (Fig. 17(d)). Presented results allow to conclude that the mass of the grain significantly affects the type of the grain movement and for selected grain mass the ATPID height should be appropriately tuned.

5.3. Influence of the excitation amplitude

The grain movement, damping ability of the ATPID and resulting displacement of the beam are also influenced by excitation parameters such as its amplitude and frequency. In particular, the paper [46] describes various types of particle displacements as a function of dimensionless acceleration factor based on the excitation amplitude. Herein, we focus on more straightforward analysis and we consider the grain movement for four different excitation amplitudes: $A_1 = 0.005$ [m], $A_2 = 0.0075$ [m], $A_3 = 0.01$ [m], $A_4 = 0.02$ [m]. In each simulation the mass of the particle is equal $m_g = 0.1M$ and constant damper height equals $h_{max} = 0.2$ [m]. Displacements of the damper floor, ceiling and grain are presented in Fig. 18.

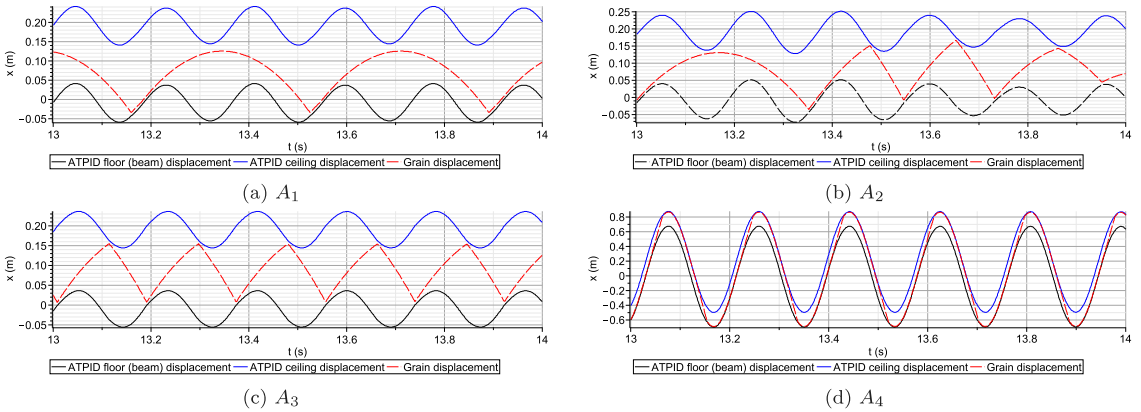

Fig. 18. Damper (floor and ceiling) and grain movement for various excitation amplitudes ($A_1 \rightarrow A_4$).

The conducted analysis shows the same types of ATPID operation as in the previously considered cases of height and grain mass influence (Fig. 15, 16, 17). For the low excitation amplitudes, the beam acceleration and resulting grain velocity at the end of the contact stage is too small to cause a grain-ceiling impact (Fig. 18(a)), or the impacts are random and unpredictable (Fig. 18(b)). In

turn, Fig. 18(c) presents the favourable situation when grain mass and damper height are appropriately adjusted to the analysed amplitude of excitation and only impacts without sticking effect are observed. Further increase of excitation amplitude causes rising of the beam acceleration and occurrence of the undesirable sticking effect between the grain and the lower or upper ATPID wall.

6. Energy analysis of the ATPID damper

In Sections 4 and 5, a description of the complicated ATPID operation and nonlinear influence of its parameters on the damping ability was presented. For a better understanding of the occurring physical phenomena, an energy analysis of the system has to be performed. The section starts with a study of grain–floor and grain–ceiling contact forces (Fig. 19), which play a key role in the system energy changes. Further, we present the complete system energy balance, in which crucial components are the change of the total beam energy (Figs. 20 and 21), the work done by the contact forces (Figs. 22 and 23) and the work done by the external excitation (Fig. 24). The section finishes with presentation of the Specific Damping Coefficient, which uses energy changes in subsequent vibration cycles to describe system damping ability (Fig. 25).

6.1. Overlaps, overlaps rates and contact forces

Grain–wall contact forces are described by the nonlinear viscoelastic contact theory and defined by Eqs. (13) and (14). The quantities which play a basic role in the description of the contact forces are grain–wall overlaps and overlaps rates arising during subsequent impacts. In the presented analysis, the overlaps, overlaps rates and contact forces were computed for five different damper heights ($h_1 \rightarrow h_5$) and presented in Fig. 19.

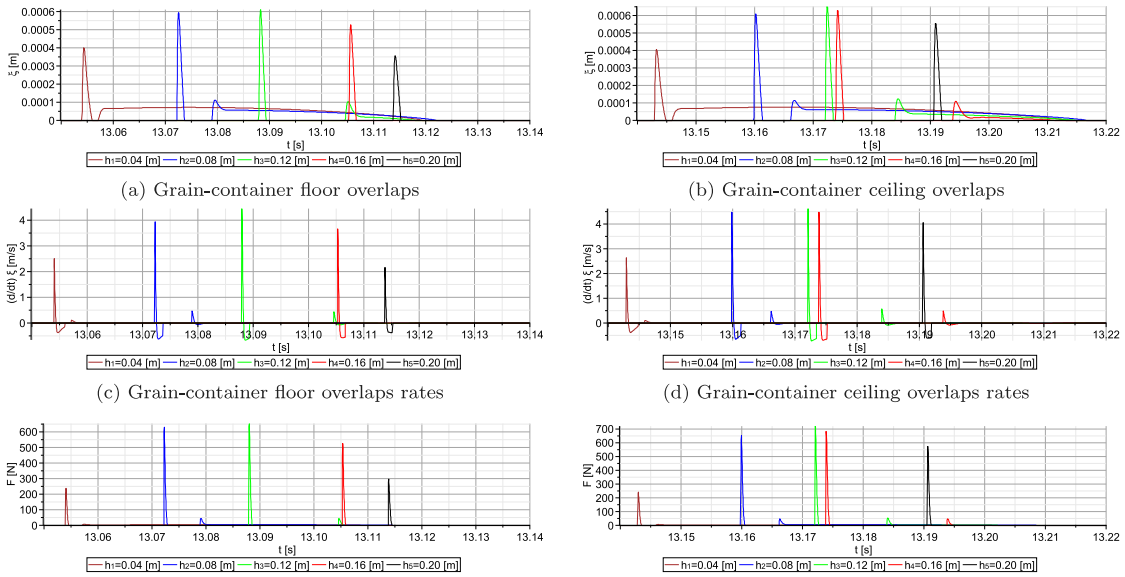

(a) Grain-container floor overlaps
(b) Grain-container ceiling overlaps
(c) Grain-container floor overlaps rates
(d) Grain-container ceiling overlaps rates
(e) Grain-container floor contact forces
(f) Grain-container ceiling contact forces

Fig. 19. Overlaps, overlaps rates and contact forces for various container height — $h_1 \rightarrow h_5$.

The plots of grain–floor and grain–ceiling overlaps are presented in Figs. 19(a) and 19(b) differ significantly for various heights of the cylinder. In both cases, two stages can be observed: the first — a short peak with high overlap amplitude, and the second — a long period when the overlap remains almost constant and further gradually decreases to zero. The first stage corresponds to the initial impact between grain and wall, which is observed in every analysed case. The second stage corresponds to the sticking effect when the grain is pushed by the container floor or ceiling (cases $h_1 \rightarrow h_4$ in Fig. 19(a) and cases $h_1 \rightarrow h_3$ in Fig. 19(b)). The grain–floor and grain–ceiling overlap rates (Figs. 19(c) and 19(d)) take positive and negative values during the initial impact and very small values during the sticking stage. The plots of contact forces (Figs. 19(e) and 19(f)) include peaks of forces of high amplitudes corresponding to the initial impact and smaller peaks corresponding to the secondary impact at the beginning of the sticking stage.

6.2. Balance of system energy

In order to reveal the impact of the contact forces on change of system energy and vibrations damping, the equations of motion (Eqs. (27) and (28)) were integrated with respect to displacements x_s and x_g to obtain the equations of global energy balance of the beam and grain:

$$\int_{\Delta x_s} m_s \ddot{x}_s \mathrm{d}x_s + \int_{\Delta x_s} F_{ext} \mathrm{d}x_s + \int_{\Delta x_s} (F_{c_1} - F_{c_2}) \mathrm{d}x_s + \int_{\Delta x_s} Q_s \mathrm{d}x_s = 0 \tag{47}$$

$$\int_{\Delta x_g} m_g \ddot{x}_g \mathrm{d}x_g - \int_{\Delta x_g} (F_{c_1} - F_{c_2}) \mathrm{d}x_g + \int_{\Delta x_g} Q_g \mathrm{d}x_g = 0 \tag{48}$$

By identifying the terms denoting change of kinetic energy and potential energy as well as work done by external excitation and contact forces, the equations of energy balance can be written in a form:

$$\Delta E_k^s - W_{F_{ext}}^s - W_{F_c}^s + \Delta E_p^s = 0 \tag{49}$$

$$\Delta E_k^g - W_{F_c}^g + \Delta E_p^g = 0 \tag{50}$$

The equation of beam energy balance the contains change of beam kinetic energy ΔE_k^s, work done by excitation force on beam displacement $\Delta W_{F_{ext}}^s$, work done by both contact forces on beam displacement $\Delta W_{F_c}^s$ and change of beam potential energy ΔE_p^s. The equation of grain energy balance the contains change of grain kinetic energy ΔE_k^g, work done by both contact forces $\Delta W_{F_c}^g$ on grain displacement and change of grain potential energy ΔE_p^g.

Summing up the equations of the beam and grain energy balance (Eqs. (49) and (50)) allows to obtain global energy balance for the entire system:

$$\Delta E_k^s + \Delta E_k^g - W_{F_{ext}}^s - W_{F_c}^s - W_{F_c}^g + \Delta E_p^s + \Delta E_p^g = 0 \tag{51}$$

Occurring in the above equation term indicating work done by contact forces on beam displacement $W_{F_c}^s$ is an additive inverse of the work done by the system due to interaction with the grain $\overline{W}_{F_c}^s$:

$$\overline{W}_{F_c}^s = -W_{F_c}^s \tag{52}$$

Moreover, the difference of work done by system due to interaction with the grain $\overline{W}_{F_c}^s$ and work done by the contact force on the grain $W_{F_c}^g$ is the total work done on the contact element and can be expressed as:

$$\overline{W}_{F_c}^s - W_{F_c}^g = D + \Delta E_p^c \tag{53}$$

where D is energy dissipation in contact element and ΔE_p^c is the change of potential energy of the contact spring, which vanishes in non-contact stage of the process. Thus, the energy balance for the whole system during the periods when the contact between ball and container wall does not appear takes a classical form:

$$\Delta E_k^s + \Delta E_k^g - W_{F_{ext}}^s + D + \Delta E_p^s + \Delta E_p^g = 0 \tag{54}$$

Comparison of Eqs. (49) and (54) reveals the difference between terms causing the change of beam energy and entire system energy. The change of beam energy is caused by work done by external force and work done by the system due to interaction with the grain. In turn, the change of the energy of the entire system is caused by work done by external excitation and dissipation occurring during grain–wall collisions.

Let us note that during the steady-state response of the system, the sum of kinetic and the potential energy of the grain remains constant after each cycle of vibrations: $\Delta E_k^g = \Delta E_p^g = 0$. Thus, according to Eq. (50), the work done by contact forces on the grain displacement equals zero: $W_{F_c}^g = 0$ and according to Eq. (53), the work done by the system due to interaction with the grain is equal to total energy dissipation in the system: $\overline{W}_{F_c}^s = D$. This implies that work done by the beam due to interaction with the grain $\overline{W}_{F_c}^s$ is always positive (similarly as the dissipation) and causes reduction of the total energy of the beam and damping of its vibrations. Furthermore, the entire energy dissipation which occurs in the system reduces the energy of the beam and does not affect the energy of the grain, which is favourable from the point of view of vibrations damping.

The selected of the above defined energy and work terms were calculated for various container heights and presented in Figs. 20–23. Due to the fact that direct numerical computation of the work done by contact forces of extremely short duration is difficult and time-consuming, they were determined by computing all other energy and work terms and assuming that Eqs. (47) and (48) are a priori fulfilled.

Fig. 20 presents changes of the summary kinetic and potential energy of the beam, which constitutes dominating part of its total energy, for various ATPID container heights. For the deactivated (closed) damper, the maximal summary kinetic and potential energy value exceeds 9 [J]. In every considered case the process of ATPID opening decreases the maximal value of system energy. For the largest considered container height h_5 the vibration damping process is the most effective and maximal summary kinetic and potential energy of the beam is below 1 [J] during the steady-state response (for $t > 12$ [s]). As previously explained, the observed process of vibrations mitigation can be attributed to changes of the system natural frequency resulting from the movement of the particle (cf. Section 4). On the other hand, such a process can be explained by the occurrence of contact forces and work done by these forces on the displacement of the beam.

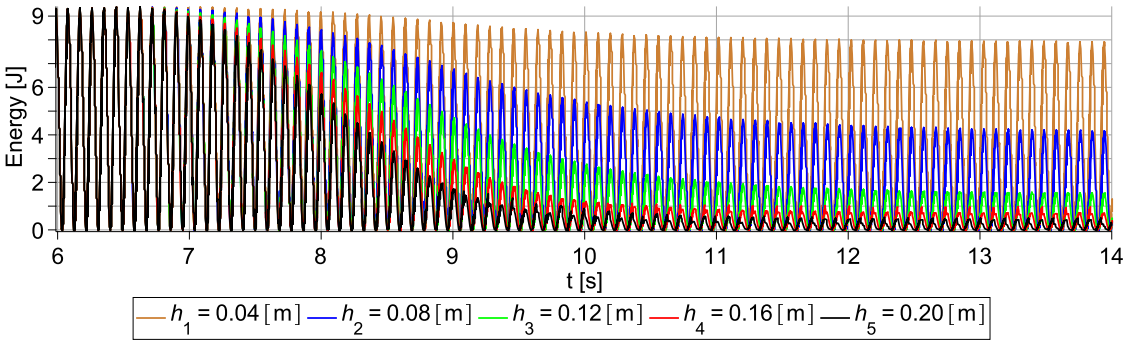

Fig. 20. Change of the beam summary kinetic and potential energy for various container heights - $h_1 \rightarrow h_5$.

According to Eq. (49), the total energy of the beam changes as a result of permanent work done by external excitation and work done by contact forces during the periods of impacts. Both mentioned work terms depend on the height of the container of the ATPID damper. In particular, the shapes of the contact forces plots are significantly different for various damper heights, as presented in Figs. 19(e) and 19(f), so work done by these contact forces on beam displacement and changes of beam kinetic energy during impacts will also vary. In order to analyse such a problem, the changes of the beam summary kinetic and potential energy during a short range of damped steady-state vibrations for five different container heights were calculated and presented in Fig. 21.

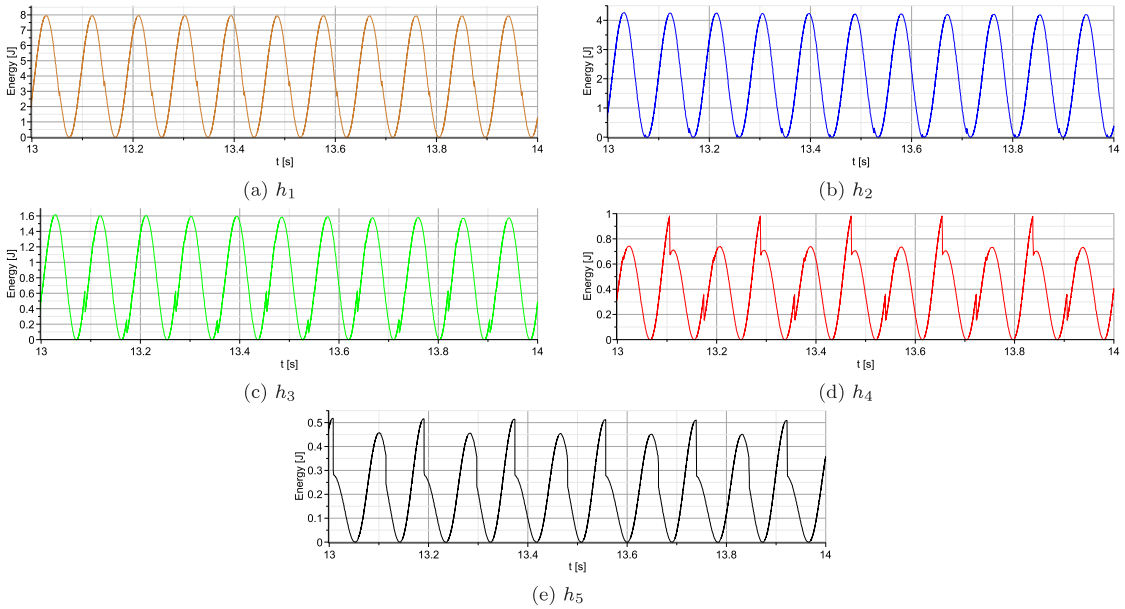

Fig. 21. Change of the beam summary kinetic and potential energy for steady state response — 13 [s] $< t <$ 14 [s].

For the case h_1, the impacts occur when the kinetic energy reaches approximately half of the maximal value in steady state. Since the direction of the contact force is the same as the direction of beam movement, the energy of the beam during the main stage of impact increases by 3.7% of the maximal amplitude. An analogical situation is observed in the case h_2 (Fig. 21(b)) in which the collisions occur when the kinetic energy of the beam is close to minimal and energy increases by 3.5%. In the next three cases (h_3–h_5) the direction of beam movement is opposite to the direction of the contact forces and thus the energy of the beam decreases in every impact. For example, for the case h_3, in which the impact to occurs when the kinetic energy is still close to the minimal one, the energy is decreased by 15% of the maximal amplitude for the upper contact force and by 12% of the maximal amplitude for the lower contact force. Further increasing of the container height causes that the impacts occur closer to the maximal value of kinetic energy and their effectiveness raises. In the case h_4 the energy is decreased by 35% and 16% of the maximal amplitude for the upper and lower impact, respectively. For the most effective case h_5, in which the impact occurs when the kinetic energy is very close to maximal, the upper contact force changes beam energy by 53% of the maximal amplitude and lower contact force — by 23% of the maximal amplitude.

The additional information is provided by analysis of the plots of work done by the system due to interaction with the grain $\overline{W}^s_{F_c}$ and work done by external excitation $\Delta W^s_{F_{ext}}$ during the entire process. In particular, Fig. 22 presents changes of work done by the system due to interaction with the grain $\overline{W}^s_{F_c}$ for various container heights.

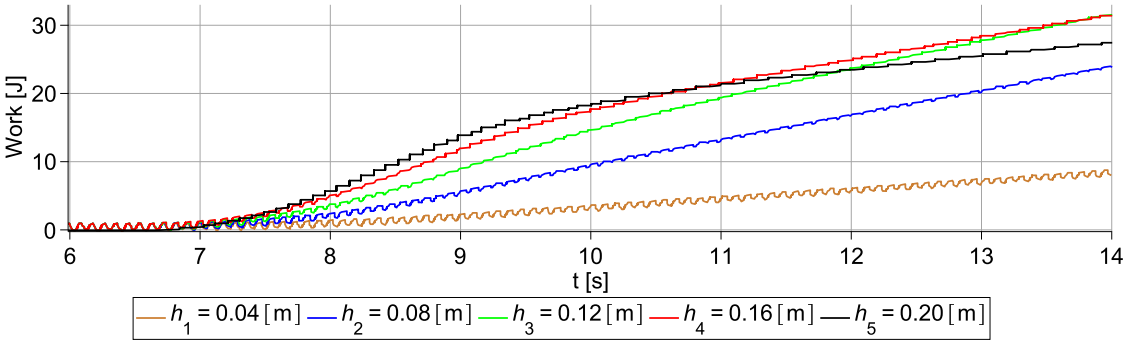

Fig. 22. Work done by the system due to interaction with the grain $\overline{W}^{s}_{F_c}$ and for various container heights — $h_1 \rightarrow h_5$.

In all considered cases the computed work $\overline{W}^{s}_{F_c}$ is always positive and gradually raises despite the fact that the occurring contact forces are entirely different for each container height. The changes of work during the process have a nonlinear form. During the first part of the process, the work done by the system increases along with the container height. Consequently, it is the largest for the optimal container height h_5, which corresponds to the smallest vibration amplitudes. However, during the second part of the process, such tendency is not maintained, and work computed for the optimal container height h_5 becomes smaller than in the other cases (h_3 and h_4).

In order to conduct a more detailed analysis, the short time plots (13 [s] $< t <$ 14 [s]) of the work done by the system due to interaction with grain are presented separately for each container height in Fig. 23. The plots in Figs. 23(a) and 23(b) correspond to the situations when the directions of the impacts are the same as the directions of beam movement. In such cases, each collision can be divided into two stages. During the main stage of the impact, the work done by the system on the grain suddenly decreases (work is done by the grain on the system), which corresponds an increase of beam kinetic energy. However, during the sticking stage, when the grain is pushed by the beam, the work done by the system increases to a value larger than before the impact. In contrast, in cases h_3–h_5 the computed work increases during each collision and causes a permanent decrease of beam kinetic energy, which is favourable from the vibrations mitigation point of view.

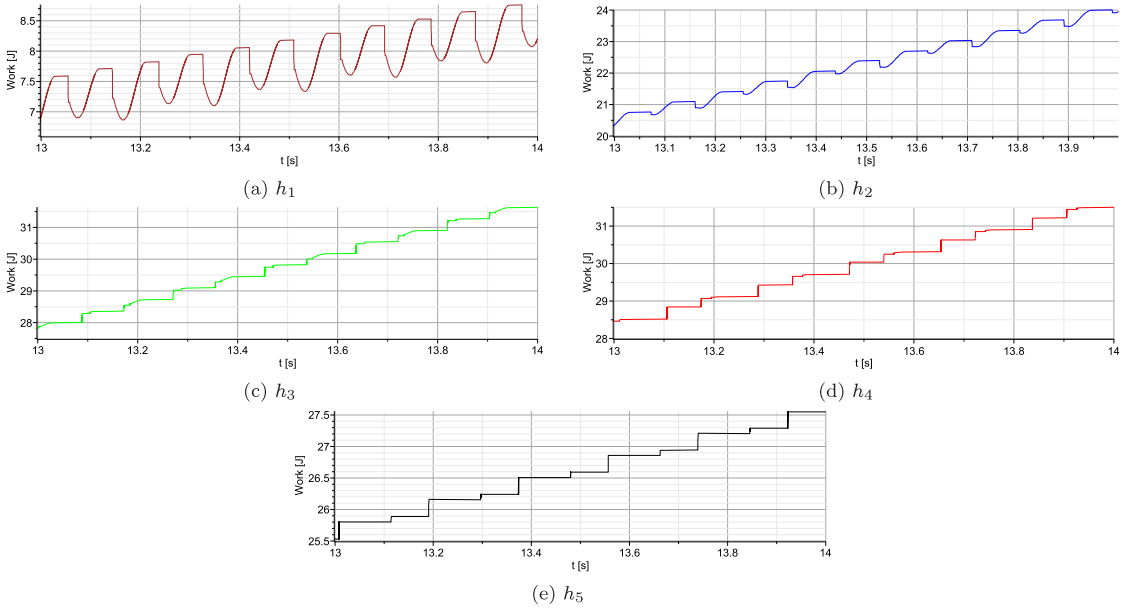

Fig. 23. Work done by the system due to interaction with the grain $\overline{W}^{s}_{F_c}$ for steady-state beam response — 13 [s] $< t <$ 14 [s].

The reason for the different effectiveness of the ATPID damper for various container heights is the different value of work done by external forces in each case. As previously explained, the change of container height results in modification of the system natural frequency, causes that the excitation frequency is out of resonance range, and reduces amplitudes and velocities of system vibrations. In order to explain the corresponding changes of system energy, the work done by excitation forces $W^{s}_{F_{ext}}$ and the work done by the system due to interaction with the grain $\overline{W}^{s}_{F_c}$ for two different container heights (h_1 and h_5) were presented in Fig. 24.

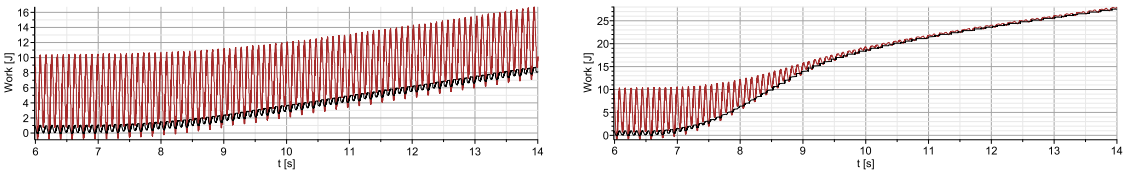

(a) h_1 (b) h_5

Fig. 24. Work done by excitation forces $W^s_{F_{ext}}$ and work done by the system due to interaction with the grain $\overline{W}^s_{F_c}$ for two container heights (h_1 and h_5).

In the situation when the height of the container is very low (h_1), the average difference between the work done by excitation forces $W^s_{F_{ext}}$ and the work done by the system due to interaction with the grain $\overline{W}^s_{F_c}$ is significant during the whole vibration process (Fig. 24(a)). It means that the change of total energy of the system depends mainly on the highly oscillating component of the work done by excitation forces. As a result, the change of the system energy is almost not observed. In the case when height of the container is properly tuned (h_5), the shift of system natural frequency causes that oscillations of the work done by excitation forces gradually decrease and they are very small when damped steady-state is obtained (Fig. 24(b)). Moreover, the work done by the system due to interaction with the grain approaches the values of the work done by excitation forces. As a result, the difference between work done by both forces is relatively low, which corresponds to small oscillations of the system energy and the effective process of beam vibration damping.

6.3. Specific damping coefficient

Specific Damping Coefficient (SDC) is a parameter which allows to describe ATPID operation characteristics [7]. It can be defined as a ratio of the energy lost $W(t_i)$ and initial energy $E(t_i)$ per one cycle of vibrations:

$$\Psi(t_i) = \frac{W(t_i)}{E(t_i)} \tag{55}$$

The energy lost within a single cycle of vibrations can be calculated as:

$$W(t_i) = E(t_i) - E(t_{i+1}) \tag{56}$$

The computations of the SDC can be simplified by analysing time instants when system velocity equals zero, the corresponding kinetic energy vanishes ($E_k = 0$) and the entire system energy is equal to the potential energy:

$$E(t_i) = \frac{kx(t_i)^2}{2} \tag{57}$$

By using Eqs. (55), (56) and (57), one obtains the final formula for the SDC:

$$\Psi(t_i) = \frac{x(t_i)^2 - x(t_{i+1})^2}{x(t_i)^2} \tag{58}$$

The changes of Specific Damping Coefficient for several cycles of beam vibrations during the unsteady state of system operation (6 [s] < t < 12 [s]) were computed for five different damper heights and presented in Fig. 25. The SDC plots reveal the change of ATPID damping ability in terms of process time and container height. The obtained results confirm once again that the damping ability for the smallest analysed container height h_1 is insignificant, while the largest damping efficiency is obtained for the container height h_5. In every case, the biggest value of SDC is observed approximately in half of the analysed damper activation period.

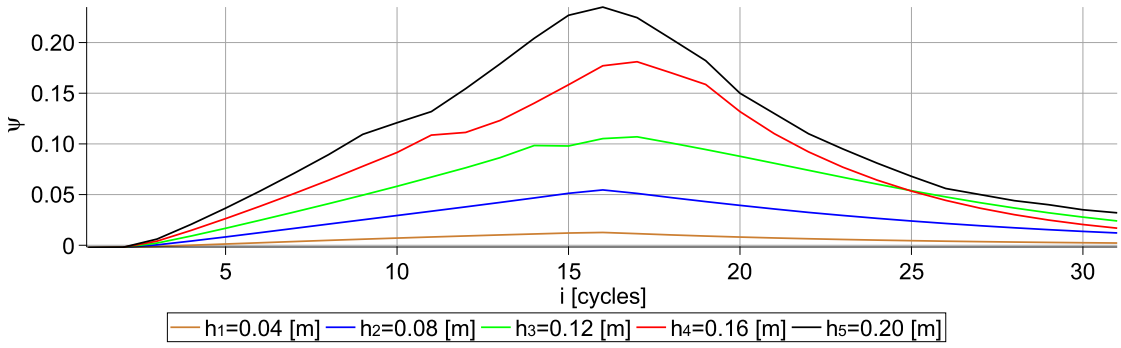

Fig. 25. Specific Damping Coefficient of vibration during unsteady state of system operation.

The SDC was also computed for the ATPID damper heights equal to $h_6 = 0.3$ [m] and $h_7 = 0.6$ [m], when the collisions between the grain and ceiling do not occur in every period of the vibrations. In such situations, the randomness of collisions causes unstable

system response with an increase and decrease of vibration amplitudes. This is reflected by irregular changes of Specific Damping Coefficients, which assume both positive and negative values.

The presented considerations prove that the appropriate choice of the damper height is crucial for the ATPID damping abilities and mitigation of the dynamic response of the considered system. This is a reason for proposing solutions in which it is possible to tune (in real time) the damper height and adapt it to the current system operation.

7. ATPID parameters optimization

In Section 5 we have presented the sensitivity of the dynamic response of the ATPID damper for three parameters: the container height, grain mass and excitation amplitude. In this section, the previously obtained results will be used to optimize amplitudes of the steady-state beam vibrations x with respect to the container height h_{max} for different values of grain mass m_g and excitation amplitudes A. A mathematical formulation of the considered optimization problem is described by Eq. (59).

$$\begin{aligned} &\text{Minimize:} && \max_{t\in(t_{min},t_{max})} x_s(A, m_g, h_{max}, t) \\ &\text{with respect to:} && h_{max} \\ &\text{subject to:} && \text{governing equations (Eqs. (27)–(29))} \\ & && A = A_i,\ (i = 1, \dots, 5) \\ & && m_g = m_i,\ (i = 1, \dots, 5) \\ & && h'_{max} < h_{max} < h''_{max} \end{aligned} \tag{59}$$

The system parameters used in numerical solution of the optimization problem are as follows: $t_{min} = 12$ [s], $t_{max} = 14$ [s] (range of damped steady-state vibrations), $h'_{max} = 0.017$ [m], $h''_{max} = 0.8$ [m] (full range of container height considered in previous sections). Moreover, the subsequent values of decreasing grain masses m_g and excitation amplitudes A are presented in Table 6.

Table 6
Parameters used in the optimization problem.

m_g [kg]	$m_1 = 0.3M$	$m_2 = 0.2M$	$m_3 = 0.1M$	$m_4 = 0.05M$	$m_5 = 0.025M$
A [m]	$A_1 = 0.03$	$A_2 = 0.02$	$A_3 = 0.01$	$A_4 = 0.005$	$A_5 = 0.0025$

The optimization problem was solved by direct search of the parameters space. The results of the conducted analysis are presented in Fig. 26, which is divided into five plots corresponding to different values of excitation amplitudes. The vertical axis of each plot presents a maximal amplitude of vibrations during ATPID damped steady-state operation for five different grain masses and a wide range of container heights.

The combination of the ATPID container height, grain mass and excitation amplitude determines the type of the ATPID operation (described in Section 5) and the resulting effectiveness of vibrations mitigation. It is expected that in the optimal solution the determined container height should provide the impact without a sticking effect and shortest possible time of grain–wall contact in every cycle of vibration. Such an optimal damper height is different for various grain masses and excitation amplitudes, see Fig. 26(a). The optimal height h_{opt} for m_1 case is equal approximately 0.2 [m], for m_2 case $h_{opt} = 0.32$ [m] and for m_3 case $h_{opt} = 0.6$ [m]. For cases m_4 and m_5, the global solution is above the upper bound of the assumed range of damper height. For the container heights lower than the optimal one, the worse damping ability is observed due to the previously described sticking effect between the grain and container walls. In turn, for the container heights higher than the optimal one, the worse damping properties are caused by the unpredictable movement of the grain without cyclic impacts against the lower and upper absorber wall. Analogical conclusions can be applied to Fig. 26(b) (cases m_1–m_5), Fig. 26(c) (cases m_2–m_5), Fig. 26(d) (cases m_3–m_5) and Fig. 26(e) (cases m_4 and m_5).

In most cases, after the optimal solution, the rumble effect is present, which causes deterioration of the system response in comparison to the optimal one. The discrepancy from this principle occurs e.g. in Fig. 26(c) for the biggest grain mass (m_1). In this solution, the optimal damper height is reached very fast and the rumble effect is almost not observed. For larger damper heights the process of damping is stabilized, which corresponds to the constant value of obtained vibration amplitude. In this case the response of the system is similar (slightly worse) as for the optimal damper height. The analogous situation is presented in Fig. 26(d) for the cases m_1 and m_2 and in Fig. 26(e) for cases m_1, m_2 and m_3. Another phenomenon can be observed in Fig. 26(e) for the case m_4, where the rumble effect occurs alternately with the constant system response.

The important and interesting feature of the proposed particle impact damper is that each combination of grain mass and excitation amplitude requires a different optimal value of container height corresponding to the minimal vibration amplitude. On the other hand, it is expected that during real-life operation, the considered mechanical system will be subjected to different dynamic excitations, which will require different optimal values of damper parameters. Such a problem requires a technical solution providing control of the damper height in a real time, which is possible thanks to the proposed ATPID construction.

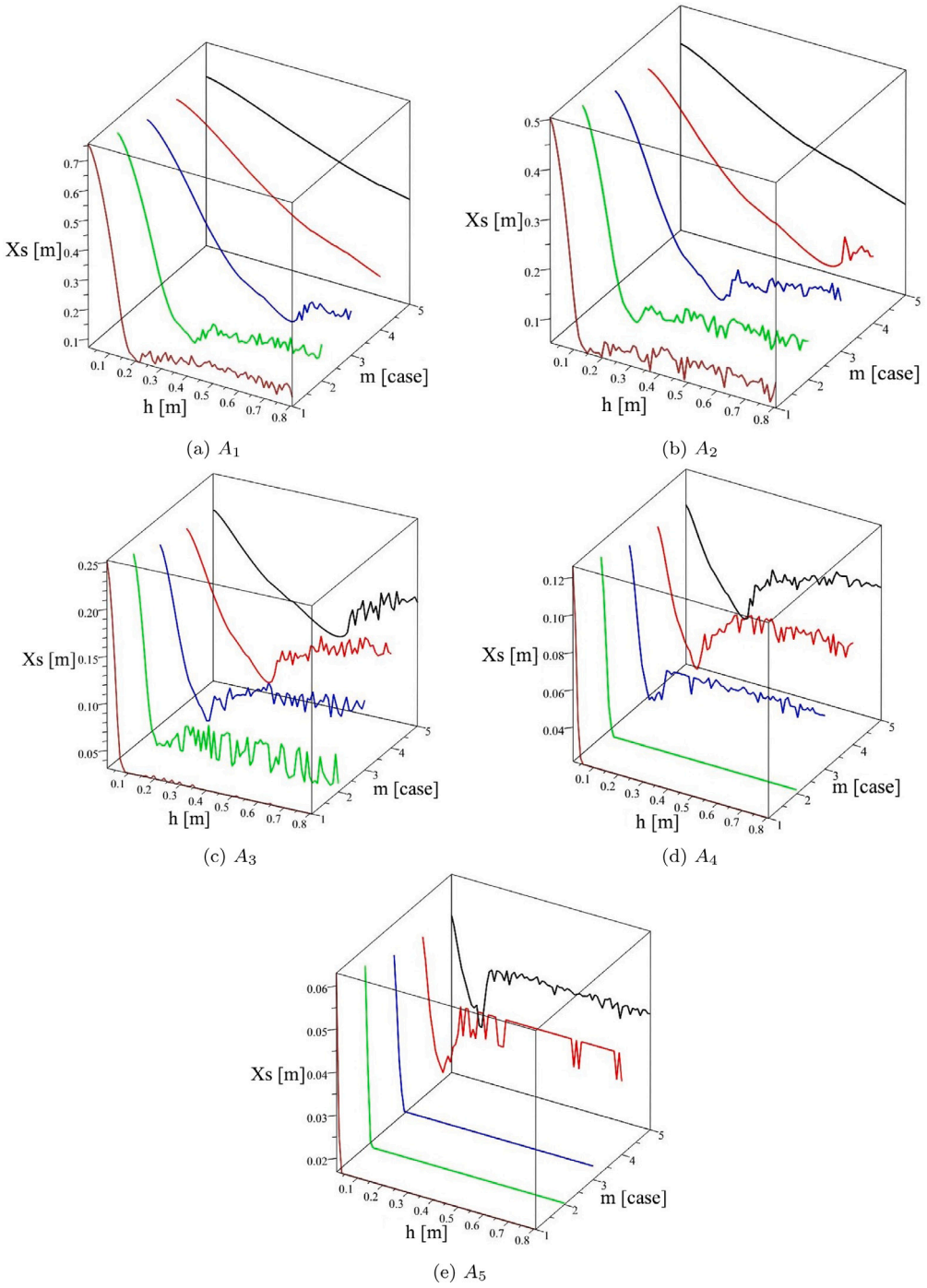

Fig. 26. Optimization of the container height for various grain mass and excitation amplitude.

In order to compare damper efficiency for different excitation amplitudes the parameter d defined as the percentage ratio of the amplitudes of damped steady-state vibrations x_s^d and undamped steady-state vibrations x_s^{ud} (when the particle cannot move inside the container) was introduced as:

$$d = |1 - \frac{x_s^d}{x_s^{ud}}| \cdot 100\% \tag{60}$$

The obtained results are presented in Fig. 27, which shows five graphs corresponding to the different mass of particle. Each of them consists of five plots of non-dimensional parameter d corresponding to various excitation amplitudes and a wide range of ATPID damper heights.

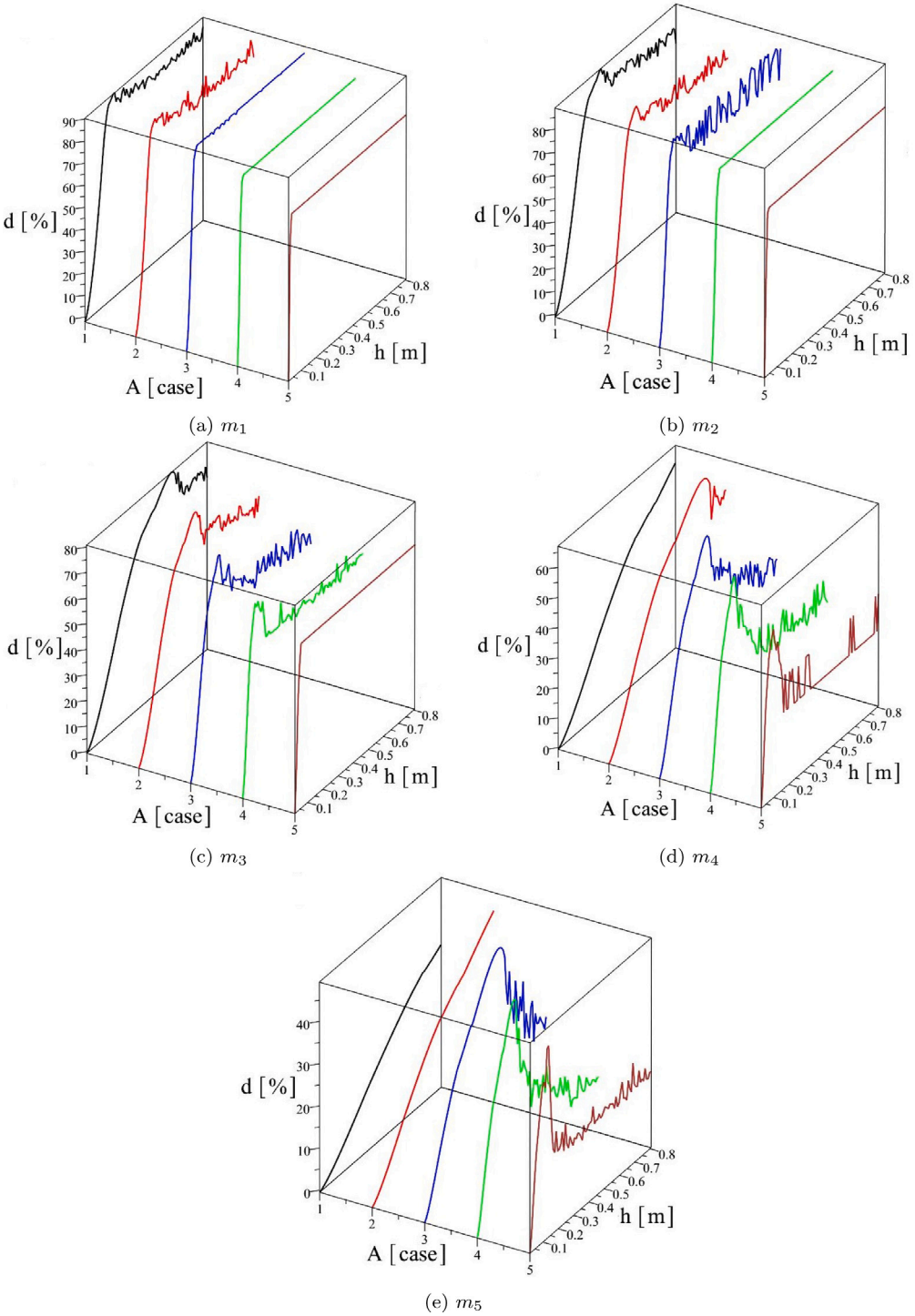

Fig. 27. ATPID damping efficiency for various container height, grain mass and excitation amplitude.

The presented plots allow to find the optimal container height and corresponding damping efficiency in relation to the excitation amplitude and grain mass. The analysis shows that for a small mass of the grain m_5 and low vibration amplitude A_5 the efficiency of vibrations mitigation is the smallest and does not reach 35%, see Fig. 27(e). Increasing the excitation amplitude results in a more effective particle movement and allows to obtain a larger efficiency of the damper ($A_5 \rightarrow A_1$ for the case m_5). Moreover, raising the grain mass causes larger values of contact forces and a gradual increase of the damper efficiency (Fig. 27(e) → Fig. 27(a)). For the highest excitation amplitude A_1 and the largest grain mass m_1 the efficiency parameter d exceeds 90%. It should be noticed that setting too large a damper height for a given excitation amplitude and grain mass might lead to rumbling and a significant decrease in the system damping ability.

Based on the results from Figs. 26 and 27, the optimal damper heights, which should be used for each combination of five different masses and five different excitation amplitudes were determined and presented in Fig. 28(a). The corresponding damping efficiencies were presented in Fig. 28(b).

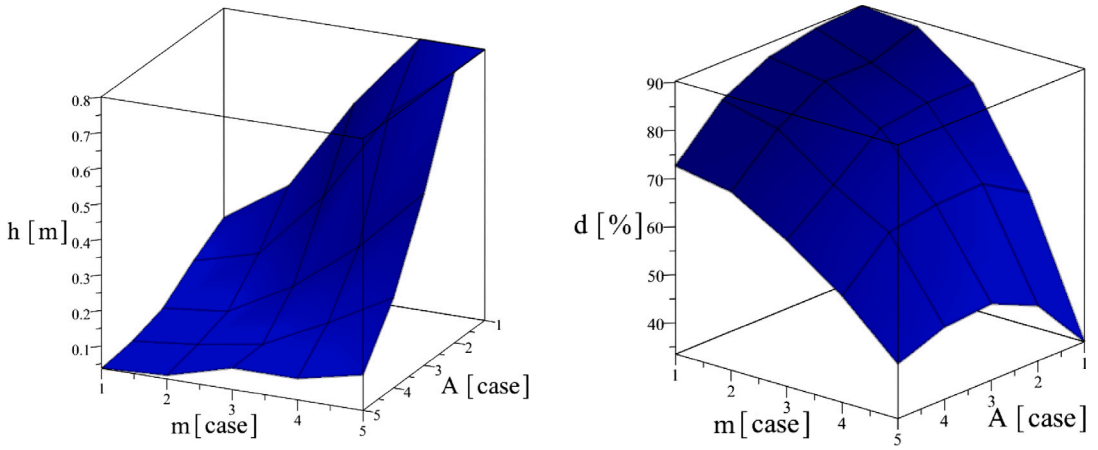

(a) Optimal container heights corresponding to various grain mass and excitation amplitudes

(b) ATPID damper efficiencies for corresponding to optimal container heights, various grain and excitation amplitudes

Fig. 28. Optimal results for various system parameters.

The analysis of the results from Fig. 28(a) allows to conclude that the increase of the excitation amplitude and the reduction of the grain mass requires a larger damper height in order to obtain maximal vibration mitigation. In turn, Fig. 28(b) shows that the highest damping efficiency is obtained for the highest excitation amplitude and the largest grain mass. The obtained theoretical results reveal that the ATPID damper enables the reduction of the resonance vibrations by up to 90%. However, it should be noticed that the optimal solution is very close to the range in which the system may fall into an undesirable rumble response.

Experimental verification

Based on Figs. 27 and 28(b) of the manuscript, it turns out that the highest efficiency of the ATPID damper in reducing beam vibrations (about 90%) was achieved when using a grain of mass equal to 30% (m_1) and 20% (m_2) of the entire system's mass, and for excitation amplitudes of $A_1 = 0.03$ [m] and $A_2 = 0.02$ [m]. Therefore, the test stand was appropriately adjusted to the above grain mass and excitation amplitudes values. The experimental tests were carried out for the cases when the damper was deactivated (i.e., the height of the damper was $h_1 = 0.017$ [m]) and for the optimally tuned damper (which is denoted as h_2 in the figure legends). Fig. 29 shows the results obtained for parameters $m_1 = 0.3M$ and A_1=0.03 [m]. The results for the remaining parameters are presented in Table 7.

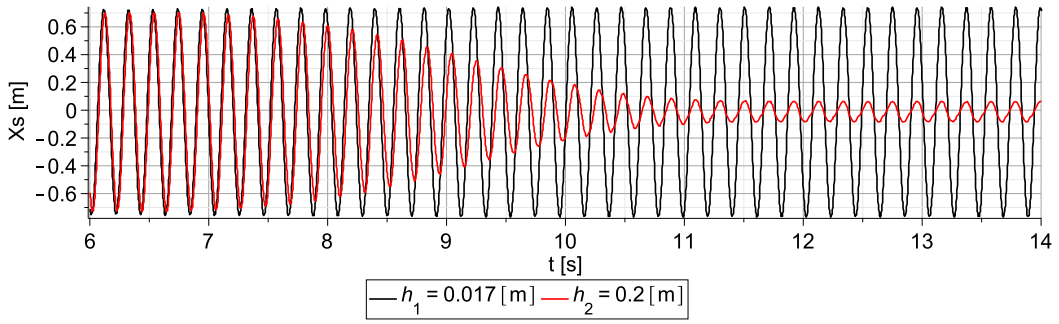

Fig. 29. Comparison of the experimental vibration amplitudes obtained in the undamped system (h_1) and in the system with optimal ATPID height (h_2) for parameter: $m_1 = 0.3M$ and $A_1 = 0.03$ [m].

Table 7
Experimental results of the undamped vibration amplitude x_s^{ud}, optimal damped vibration amplitude x_s^d and ATPID damper efficiency d for various grain mass m_g and excitation amplitudes A.

m_g	A [m]	x_s^{ud} [m]	x_s^d [m]	d [%]
m_1=0.3M	A_1=0.03	0.745	0.065	91.4
m_1=0.3M	A_2=0.02	0.493	0.043	91.3
m_2=0.2M	A_1=0.03	0.698	0.064	90.8
m_2=0.2M	A_2=0.02	0.462	0.052	88.7

Upon comparing the results of the experimental tests (Fig. 29 and Table 7), it can be observed that the amplitude of beam vibrations in a damped steady state x_s^{ud} is reduced by approximately 90% compared to the beam response in resonance vibrations x_s^d (when the damper is deactivated). The experimental tests provide strong evidence for the accuracy of the proposed numerical model and validate the results obtained from the numerical analyses presented in Figs. 26–28.

8. Real-time control strategy for ATPID

The obtained results of experimental tests, numerical simulations and optimization processes constitute the basis for the development of real-time control strategies, which provide an adaptation of the ATPID damper to the actual working conditions and improve a vibrations mitigation process. In particular, the control strategy can be aimed at real-time adaptation of the damper height to the kinematic excitation changing amplitude. This section includes description of such a control strategy and numerical examples showing its effectiveness of mitigation of steady-state vibrations.

8.1. General concept of the control strategy

The proposed real-time control strategy for the system subjected to a kinematic excitation of changing amplitude is based on a simple feedback control loop, which is activated multiple times during the vibration mitigation process and repeatedly sets the optimal value of the damper height. In the simplest case, the feedback signal for the control loop is a measured kinematic excitation and amplitude of its resonant frequency determined using FFT analysis while the output is the optimal value of the damper height which provides a minimal amplitude of the system steady-state vibrations.

The results obtained during the holistic analysis of the ATPID damper can be effectively used for the determination of the optimal container height for the identified excitation amplitude value. In particular, two types of control system operations can be considered:

- It can be assumed that the optimal damper heights corresponding to the expected range of excitation amplitudes are a priori determined before the vibration mitigation process and stored in the memory of the hardware controller. In such a case obtained from the conducted optimization procedure surface [A, m, h] (Fig. 28(a)) can be used as a look-up table for selecting the optimal container height for an actual amplitude of kinematic excitation.
- It can be assumed that the optimal damper height is not a priori known parameter and has to be determined during the vibration mitigation process. In such a case the process of finding an optimal value can utilize previously determined fundamental properties of the system reflected in dependencies between the damper height and the vibration amplitude (Fig. 26) or the damping percentage ratio (Fig. 27), especially the fact that the optimal height is the largest one for which the rumbling effect does not occur. On the other hand, the optimization for a subsequent excitation amplitudes can effectively utilize the shape of surface [A, m, h], which reveals that optimal damper height depends monotonically, but non-linearly on the excitation amplitude.

Eventually, the proposed control system (Fig. 30) utilizes a single feedback control loop and it is composed of the following components:

- block for the on-line measurement or identification of the actual amplitude of the applied kinematic excitation;
- block for determination of the optimal container height corresponding to the identified excitation amplitude based on: (i) pre-computed look-up table containing the set of optimal container heights for given grain mass and expected excitation amplitudes or (ii) on-line optimization/direct search algorithm utilizing fundamental properties of the analysed system.
- block for generation of the voltage signal for the electric engine.
- block of the electric engine which provides that the appropriate height of the container is set.

The input for the control loop is a selected component of the actual response of the system. Typically, it can be the amplitude of the beam vibration, which can be effectively used for identification of the external excitation amplitude. In turn, the output from the control loop is optimal height container height, which is set by the applied engine using optimal voltage signal. The input to the entire system equipped with ATPID consists of external excitation and optimal container height obtained as a result of the execution of the control loop. Both these quantities contribute to the dynamic response of the system.

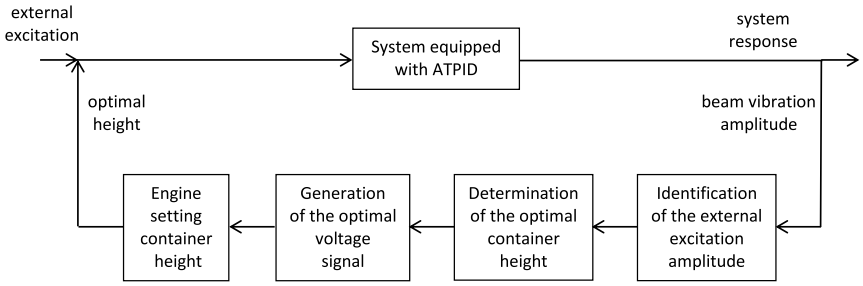

Fig. 30. General scheme of the proposed control system.

The application of the above feedback control loop is repeated multiple times during the vibration mitigation process when the measurement system detects change in the excitation amplitude (or its change exceeds a certain threshold). Such a process ensures the optimal real-time tuning of the container height, adaptive operation of the ATPID damper and an effective mitigation of the steady-state vibrations.

8.2. Numerical simulations of real-time control algorithm

The presented numerical example shows the application of the above proposed real-time control algorithm for adaptation of the ATPID height to actual operational conditions. The example reveals the effectiveness of the control algorithm in the mitigation of a steady-state vibrations caused by harmonic kinematic excitation of variable, time-dependent amplitude.

The amplitude of applied kinematic excitation assumes three different values during the analysed vibration mitigation process (Fig. 31). During the first 0.5 [s] the excitation linearly increases to 0.15 [m] and reaches a constant value during 0.5–6 [s], during the following 2 [s] it linearly increases to 0.04 [m], during the time period 8–13 [s] it is maintained at a constant level of 0.04 [m], during the 1 [s] it linearly decreases to 0.03 [m], while during the final time period 14–20 [s] it is maintained constant at a constant level of 0.03 [m].

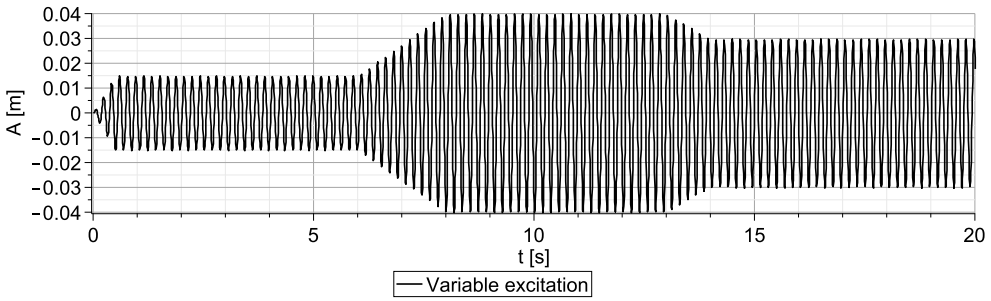

Fig. 31. Change of the amplitude of applied kinematic excitation.

The displacement of the system with a closed ATPID damper (container height equal to the grain size) is presented in Fig. 32. It can be observed that the initial steady-state of system response is reached after approximately 4 [s] and the corresponding displacement amplitude exceeds 0.3 [m]. The second steady-state is reached approximately at time instant 13 [s] and corresponding displacement amplitude reaches 0.85 [m]. Eventually, the final steady-state is obtained also approximately at 17 [s] of the simulation and the corresponding displacement amplitude exceeds 0.65 [m].

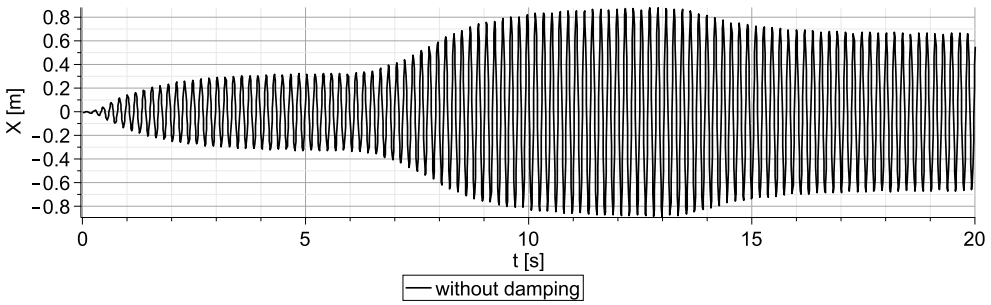

Fig. 32. Displacement of the system with closed ATPID damper.

In the following numerical simulations, the implemented real-time control algorithm adapts the actual height of the damper according to the measured or identified amplitude of the kinematic excitation. It is assumed that the precise measurement or the identification of excitation requires at least two cycles of vibrations. The optimal value of the damper height is determined on-line during the process of vibration mitigation and it is based on iterative simulations of the system response for various container heights. It is assumed that the process of searching the optimal height is relatively short in comparison to the considered time of vibrations mitigation process. The process of changing the damper height has a constant velocity and the time to reach the optimal height is shorter than time necessary to identify the excitation. The values of determined optimal damper heights for identified amplitudes constitute the reference points, which are used to determine subsequent optimal heights. In addition, when the change of excitation amplitude is not detected, the process of searching the optimal container height is continued for expected excitation amplitudes values, which allows to create and gradually expand the data base containing the set of optimal damper heights.

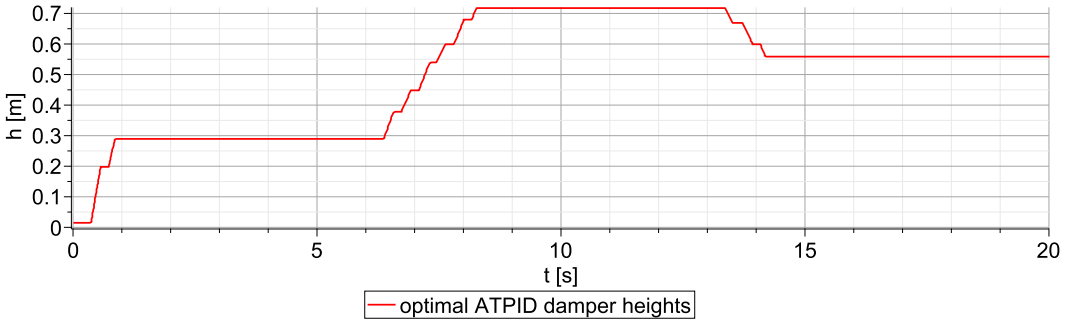

Fig. 33. Change of the damper height obtained by application of real-time control algorithm.

Comparison of the vibration amplitudes obtained in the system with a closed ATPID damper and the system with implemented real-time control strategy of container height is presented in Fig. 34. It can be observed that for the first excitation amplitude, the optimal damper height (Fig. 33) reaches 0.3 [m] and results in amplitude of steady-state vibrations of approximately 0.07 [m], for the second excitation amplitude, the optimal damper height is equal above 0.7 [m] and the response amplitude reaches above 0.17 [m], and for the third excitation amplitude, the amplitude of vibration is 0.13 [m] for the container height equal 0.57 [m]. Thus, it can be concluded that the obtained amplitudes of vibrations constitute less than 20% of the amplitudes of the undamped system. This confirms a high efficiency of the proposed adaptive system and the proposed real-time control algorithm.

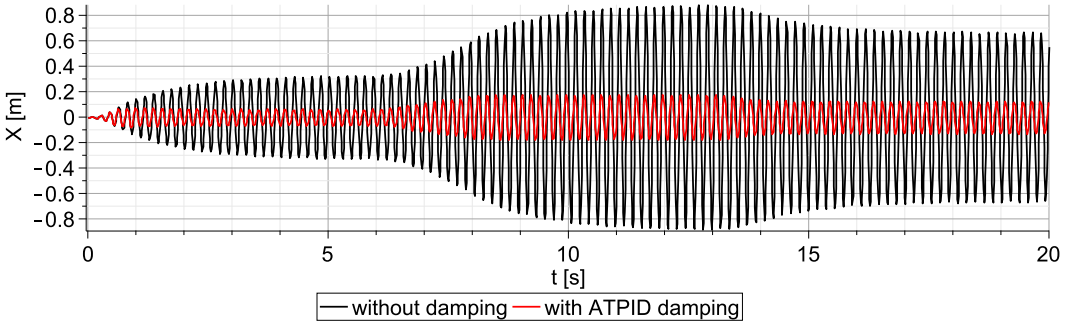

Fig. 34. Comparison of vibration amplitudes obtained in the undamped system (black) and in the system with real-time control algorithm (red). (For interpretation of the references to colour in this figure legend, the reader is referred to the web version of this article.)

The automatic method requires a hardware implementation of the proposed real-time control algorithm, which constitutes a separate research challenge and is planned in the next stage of the system development. The fully developed system will include the dedicated measurement system, hardware controller (e.g. NI Compact Rio) and currently applied controllable electric engine. The dedicated measurement system will consist of measurement cards, accelerometers and laser sensors used for the measurement of system kinematics as well as software enabling data preprocessing such as filtration and Fast Fourier's Transform. The hardware controller will collect and save the measurement data in order to identify time–history of external excitation and determine the actual value of excitation amplitude. In the next step, it will use one of the above proposed methods to determine the optimal damper height corresponding to identified excitation amplitude, and will generate the appropriate control signal for the engine. Finally, the engine will change the damper height in real-time providing adaptation of the system to changing excitation and efficient mitigation of system vibrations.

Experimental verification

The experimental tests were conducted in order to validate the proposed control algorithm with the numerical analyses considering the real-time change of excitation amplitude. In the presented numerical example, each change in excitation value was implemented linearly, leading to successive amplitudes of 0.015 [m], 0.04 [m], and 0.03 [m] (Fig. 31). However, due to limitations of applied equipment, it was not feasible to precisely replicate the above numerical approach. Therefore, the research equipment was modified to enable a stepped change in excitation amplitude, resulting in values of 0.03 [m], 0.02 [m], and 0.01 [m]. An example of the experimentally measured excitation amplitude is presented in Fig. 35.

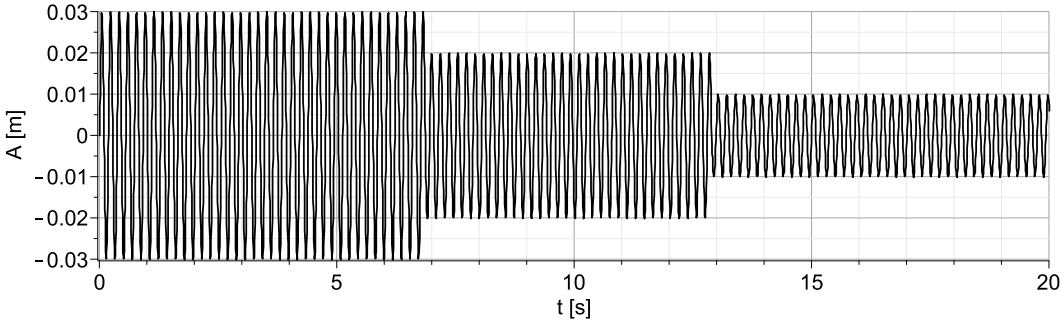

Fig. 35. Change of excitation amplitude applied in the experiment.

For the assumed range of external excitation amplitude from 0.05 [m] to 0.5 [m] the optimal damper heights were identified using the described control algorithm. During the computations 101 discrete values of excitation amplitudes varying by 0.0045 [m] and three different grain masses equal to 30% (case 1), 20% (case 2), and 10% (case 3) of the total system mass, were assumed. Therefore, three values of the optimal damper height were determined for each discrete value of excitation amplitude. This allowed for the development of a look-up table with data that was implemented into the Arduino Mega 2560 microcontroller.

During the experimental tests, the measuring system based on laser displacement sensor recorded the applied kinematic excitation and the response of the free end of the beam in real time. The results were successively saved in the microcontroller's memory, which analysed the input signal, identified the excitation amplitude, and read the optimal value of the container height corresponding to the closest value of pre-recorded amplitude from the previously implemented look-up table. Then, the Arduino controlled the electric motor responsible for setting the position of the upper wall of the damper in order to achieve the optimal ceiling position. As a result, the control strategy for the ATPID damper was implemented and tested for each of the three cases of grain mass. The real-time change of the ceiling position during the experimental tests is presented in Fig. 36.

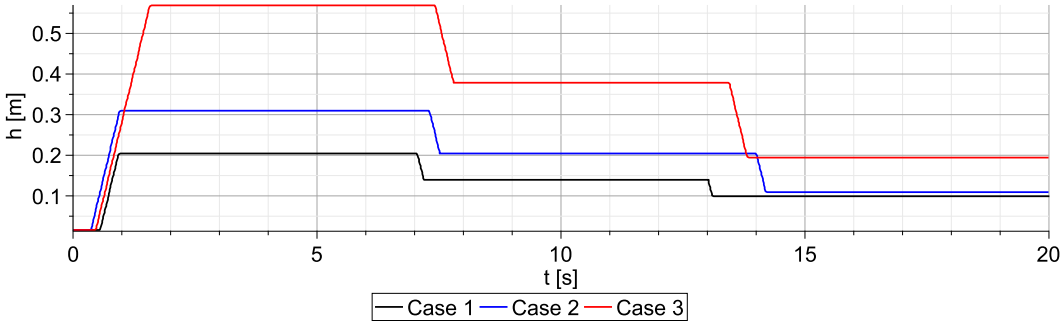

Fig. 36. Experimental implementation of the ATPID damper control strategy for three different grain mass (cases).

The analysis of the experimental results of the ATPID control strategy presented in Fig. 36 revealed different optimal values of the damper height for each measured amplitude and particle mass value. Since the electric motor was powered by a constant current during the control process, the rate of change in damper height was constant. Differences in initiation time for each stage of damper opening or closing were also observed. This was mainly due to two reasons: the lack of identical changes in excitation amplitude in the subsequent experimental tests, and the different time required for the Arduino to identify the excitation amplitude and optimal damper height. The presented control strategy resulting in optimal system damping was applied for each mass case, and the corresponding displacement of the beam end was measured. Additionally, the experiments were performed for the case of deactivated damper in which the height during the entire vibration process was minimal, resulting in resonant vibrations. The obtained results were compared and presented in Fig. 37 for case 1, Fig. 38 for case 2, and Fig. 39 for case 3.

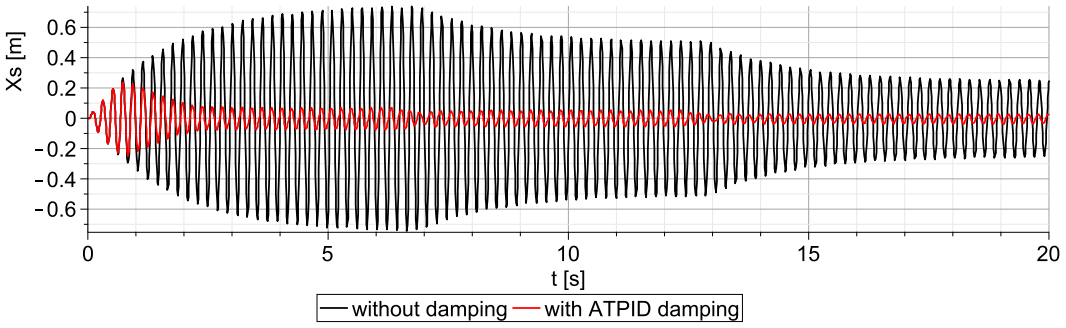

Fig. 37. Comparison of measured responses of the beam vibrations for the case 1 ($m_g = 0.3M$).

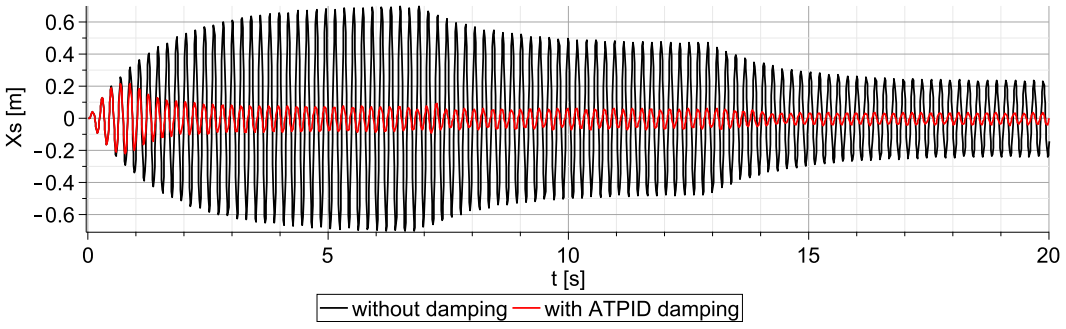

Fig. 38. Comparison of measured responses of the beam vibrations for the case 2 ($m_g = 0.2M$).

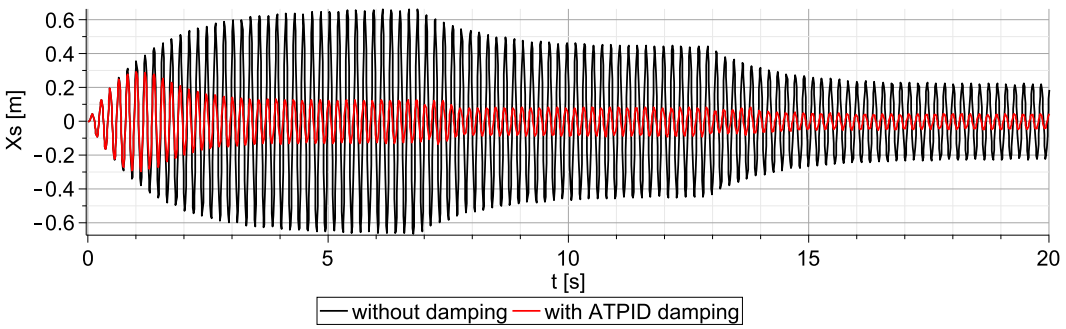

Fig. 39. Comparison of measured responses of the beam vibrations for the case 3 ($m_g = 0.1M$).

Figs. 37–39 demonstrate that the conducted experimental verification allows for real-time control of the ATPID damper, thus enabling adaptation and ensuring maximum reduction of beam vibrations for dynamically changing excitation amplitudes (Fig. 35). As a result, resonant vibrations were reduced by approximately 90% for the case 1 ($m_g = 0.3M$). For the case 2 ($m_g = 0.2M$), the vibration amplitude was attenuated by 89% for the largest excitation amplitude and by 85% for the smallest one. The lowest efficiency in reducing beam vibrations was observed in the case 3 ($m_g = 0.1M$), where resonant vibrations were mitigated by approximately 80% throughout the beam's vibrations process. These results confirm the very high effectiveness of the ATPID damper described by previous numerical and experimental analyses. The above studies of the control algorithm provide promising foundations for developing control algorithms which will enable faster and more efficient identification of the optimal damper heights.

9. Conclusions

Adaptive Tuned Particle Impact Damper (ATPID) is an innovative type of attenuator, which consists of granular material enclosed in the container of controllable size. It allows for real-time tuning of the damping characteristics and effective adaptation to the actual dynamic excitation. Development of the efficient methodology for the design of ATPID damper requires elaboration of a mathematical model based on soft contact theory and grain physical properties, an pplication of optimization techniques in order to find the required parameters, a corresponding real-time control strategy and an experimental validation of the entire system.

In this paper, the authors have proposed a simple prototype of the ATPID with a single particle and controllable height of the container. As a first step, the method of the ATPID modelling based on soft-contact theory and enhanced Hertzian contact model has been developed. It has been proved that the proposed model enables accurate simulation of the damper's influence on the mitigation of the vibrating system response by obtaining satisfactory agreement with the conducted experimental tests. The developed mathematical model reveals the fundamental principles of the ATPID operation, which include the mass modification effect and the pseudo-inertial force effect. The conducted sensitivity analysis discloses that increase of the container height and grain mass, as well as decrease of the excitation amplitude, cause a gradual change of grain movement type from the permanent sticking of the grain to container walls through the short cyclic impacts (the most efficient for vibration mitigation) to the random grain motion with irregular impacts. In addition, the quantitative analyses of the changes of system energy, work done by contact forces and external excitation indicate that the container height is the most important ATPID parameter and reveals the desired range of its changes.

According to conducted analyses, the optimal container height which provides the most efficient mitigation of steady-state vibration approximately equals to the largest height for which the rumbling effect does not occur. The ATPID absorber with the optimal container height has the following features: (a) the impacts occur when the velocity of the primary system is not necessarily maximal; (b) the velocities of the colliding masses are opposite during the impacts, but stabilization of system motion is observed both in the case when the velocities are the same and opposite; (c) the collisions occur in every period of vibrations since otherwise the random particle motion causes rumble vibrations of the entire system; (d) sticking effect between particle and container walls does not occur. Moreover, the solution of the set of optimization problems aimed at minimization of vibration amplitudes for various grain masses and excitation amplitudes discloses monotonic but non-linear change of the optimal container height in terms of these two parameters. For the largest considered grain mass and excitation amplitude, the ATPID damper is found to be extremely efficient and to reduce the amplitudes of resonance vibrations by 90%. Eventually, the obtained results allow to develop a real-time control strategy for the ATPID damper, which is based on application of the feedback control loop providing repetitive identification of the kinematic excitation amplitude and setting the optimal container height. The conducted numerical simulations reveal high efficiency of the proposed real-time control strategy in mitigation of vibration caused by continuously changing kinematic excitation and therefore prove the superiority of the proposed ATPID damper.

The proposed improvements and presented investigations eliminate the disadvantages of the classical PID dampers and prove that the proposed concept of the ATPID is both feasible and effective. The progress in PID design is obtained by the application of the real-time control component, which is still innovative in this particular type of structure. The proposed approach can be executed by application of the mechatronic system which could provide real-time modification of the container height and adaptation of damper operation to rapidly changing dynamic excitation. The conducted study significantly contributes to the increase of PID dampers functionality and their prospective application as alternative vibrations mitigation devices in various engineering environments.

CRediT authorship contribution statement

Mateusz Żurawski: Conceptualization, Methodology, Data curation, Writing – original draft, Visualization, Investigation. **Cezary Graczykowski:** Conceptualization, Methodology, Software, Data curation, Writing – original draft, Investigation, Supervision. **Robert Zalewski:** Conceptualization, Supervision, Writing – review & editing.

Declaration of competing interest

The authors declare that they have no known competing financial interests or personal relationships that could have appeared to influence the work reported in this paper.

Data availability

Data will be made available on request

Acknowledgement

The support of the National Science Centre, Poland, granted through the agreement 2018/31/D/ST8/03178 is gratefully acknowledged.

References

[1] Z. Lu, et al., Nonlinear dissipative devices in structural vibration control: A review, J. Sound Vib. (2018) http://dx.doi.org/10.1016/j.jsv.2018.02.052.
[2] L. Gagnon, M. Morandini, G. Ghiringhelli, A review of particle damping modeling and testing, J. Sound Vib. (2019) http://dx.doi.org/10.1016/j.jsv.2019.114865.
[3] B. M.Shah, et al., Semi-active particle-based damping systems controlled by magnetic fields, J. Sound Vib. (2011) http://dx.doi.org/10.1016/j.jsv.2010.08.009.
[4] M. Trigui, E. Foltete, N. Bouhaddi, Prediction of the dynamic response of a plate treated by particle impact damper, J. Mech. Eng. Sci. (2014) http://dx.doi.org/10.1177/0954406213491907.
[5] A. Afsharfard, Application of nonlinear magnetic vibro-impact vibration suppressor and energy harvester, Mech. Syst. Signal Process. 98 (2018) 371–381, http://dx.doi.org/10.1016/j.ymssp.2017.05.010.
[6] M.B. Romdhanea, et al., The loss factor experimental characterisation of the non-obstructive particles damping approach, Mech. Syst. Signal Process. (2012) http://dx.doi.org/10.1016/j.ymssp.2013.02.006.
[7] B.M. Shah, et al., Construction and characterization of a particle-based thrust damping system, J. Sound Vib. 326 (2009) 489–502, http://dx.doi.org/10.1016/j.jsv.2009.06.007.
[8] W. Liu, G. Tomlinson, J. Rongong, The dynamic characterisation of diskgeometry particle dampers, J. Sound Vib. 280 (2005) 49–861, http://dx.doi.org/10.1016/j.jsv.2003.12.047.
[9] H. Pourtavakoli, E.J. Parteli, T. Pöschel, Granular dampers: does particle shape matter? New J. Phys. (2016) http://dx.doi.org/10.1088/1367-2630/18/7/073049.
[10] K.F. Malone, B.H. Xu, Determination of contact parameters for discrete element method simulations of granular systems, Particuology (2008) http://dx.doi.org/10.1016/j.partic.2008.07.012.
[11] M. Sanchez, L.A. Pugnaloni, Effective mass overshoot in single degree of freedom mechanicalsystems with a particle damper, J. Sound Vib. 330 (2011) 5812–5819, http://dx.doi.org/10.1016/j.jsv.2011.07.016.
[12] A.D. Renzo, F.P.D. Maio, Comparison of contact-force models for the simulation of collisions in DEM-based granular flow codes, Chem. Eng. Sci. (2004) http://dx.doi.org/10.1016/j.ces.2003.09.037.
[13] C. Thornton, S.J. Cummins, P.W. Cleary, An investigation of the comparative behaviour of alternative contact force models during inelastic collisions, Powder Technol. (2013) http://dx.doi.org/10.1016/j.powtec.2012.08.012.
[14] Y. Du, S. Wang, Modeling the fine particle impact damper, Int. J. Mech. Sci. 52 (7) (2010) 1015–1022, http://dx.doi.org/10.1016/j.ijmecsci.2010.04.004.
[15] P. Eshuis, et al., Granular leidenfrost effect: Experiment and theory of floating particle clusters, Phys. Rev. Lett. 95 (2005) http://dx.doi.org/10.1103/PhysRevLett.95.258001.
[16] K. Zhang, et al., Motion mode of the optimal damping particle in particle dampers, J. Mech. Sci. Technol. 30 (2016) 1527–1531, http://dx.doi.org/10.1007/s12206-016-0305-4.
[17] H. Kruggel-Emden, et al., Review and extension of normal force models for the Discrete Element Method, Powder Technol. (2007) http://dx.doi.org/10.1016/j.powtec.2006.10.004.
[18] J. Shafer, S. Dippel, D. Wolf, Force schemes in simulations of granular materials, J. Physique I (1996) http://dx.doi.org/10.1051/jp1:1996129.
[19] J. Lee, H.J. Herrmann, Angle of repose and angle of marginal stability: molecular dynamics of granular particles, J. Phys. A: Math. Gen. (1992) http://dx.doi.org/10.1088/0305-4470/26/2/021.
[20] G. Kuwabara, K. Kono, Angle of repose and angle of marginal stability: molecular dynamics of granular particles, Japan. J. Appl. Phys. (1987) http://dx.doi.org/10.1143/JJAP.26.1230.
[21] Y. Tsuji, T. Tanaka, T. Ishida, Lagrangian numerical simulation of plug flow of cohesionless particles in a horizontal pipe, Powder Technol. (1992) http://dx.doi.org/10.1016/0032-5910(92)88030-L.
[22] D. Rodak, et al., Possibilities of vacuum packed particles application in blast mitigation seat in military armored vehicles, Bull. Pol. Acad. Sci. Tech. Sci. (2021) http://dx.doi.org/10.24425/bpasts.2021.138238.
[23] O.R. Walton, R.L. Braun, Viscosity, granulartemperature, and stress calculations for shearing assemblies of inelastic, frictional disks, J. Rheol. (1986) http://dx.doi.org/10.1122/1.549893.
[24] G. Kuwabara, K. Kono, Restitution coefficient in a collision between two spheres, Japan. J. Appl. Phys. (1987) http://dx.doi.org/10.1143/JJAP.26.1230.
[25] X. Huang, et al., Equivalent model and parameter analysis of non-packed particle damper, J. Sound Vib. (2021) http://dx.doi.org/10.1016/j.jsv.2020.115775.
[26] X. Huang, X.L.J. Wang, Optimal design of inerter-based nonpacked particle damper considering particle rolling, Earthq. Engng. Struct. Dyn. (2021) http://dx.doi.org/10.1002/eqe.3430.
[27] W. Yan, B. Wang, H. He, Research of mechanical model of particle damper with friction effect and its experimental verification, J. Sound Vib. (2019) http://dx.doi.org/10.1016/j.jsv.2019.114898.
[28] K. Zhang, et al., Experimental studies of tuned particle damper: Design and characterization, Mech. Syst. Signal Process. (2018) http://dx.doi.org/10.1016/j.ymssp.2017.06.007.
[29] C. Snoun, M. Trigui, Design parameters optimization of a particles impact damper, Int. J. Interact. Des. Manuf. (2018) http://dx.doi.org/10.1007/s12008-018-0463-y.
[30] X. Lei, C. Wu, Optimizing parameter of particle damping based on (Leidenfrost) effect of particle flows, Mech. Syst. Signal Process. 104 (2018) http://dx.doi.org/10.1016/j.ymssp.2017.10.037.
[31] R. Zhang, et al., Parametrical optimization of particle dampers based on particle swarm algorithm, Appl. Acoust. 160 (2020) http://dx.doi.org/10.1016/j.apacoust.2019.107083.
[32] L. Chung, et al., Optimal design formulas for viscous tuned mass dampers in wind-excited structures, Struct. Control Health Monit. (2011) http://dx.doi.org/10.1002/stc.496.
[33] S. Elias, V. Matsagar, Research developments in vibration control of structures using passive tuned mass dampers, Annu. Rev. Control (2017) http://dx.doi.org/10.1016/j.arcontrol.2017.09.015.
[34] J. Chen, et al., Experimental research on design parameters of basin tuned and particle damper for wind turbine tower on shaker, Struct. Control Health Monit. 2440 (2019) http://dx.doi.org/10.1002/stc.2440.
[35] W. Xiao, et al., Influence of particle damping on ride comfort of mining dump truck, Mech. Syst. Signal Process. 136 (2020) http://dx.doi.org/10.1016/j.ymssp.2019.106509.
[36] M. Heckel, et al., Granular dampers for the reduction of vibrations of an oscillatory saw, Physica A 391 (2012) http://dx.doi.org/10.1016/j.physa.2012.04.007.
[37] W. Xiao, et al., Research on vibration reduction characteristics of continuum and noncontinuum system on coupling for high-power gear transmission based on particle damping materials, Shock Vib. (2021) http://dx.doi.org/10.1155/2021/8845526.
[38] Z. Lu, et al., Experimental and analytical study on the performance of particle tuned mass dampers under seismic excitation, Earthq. Eng. Struct. Dyn. 2826 (2016) http://dx.doi.org/10.1002/eqe.2826.

[39] Z. Lu, et al., Experimental studies of the effects of buffered particle dampers attached to a multi-degree-of-freedom system under dynamic loads, J. Sound Vib. (ISSN: 0022460X) 331 (2012) 2007–2022, http://dx.doi.org/10.1016/j.jsv.2011.12.022.
[40] M. Żurawski, B. Chiliński, R. Zalewski, Concept of an adaptive-tuned particles impact damper, J. Theoret. Appl. Mech. (2020) http://dx.doi.org/10.15632/jtam-pl/122431.
[41] M. Żurawski, R. Zalewski, Damping of beam vibrations using tuned particles impact damper, Appl. Sci.-Basel (2020) http://dx.doi.org/10.3390/app10186334.
[42] S.F. Masri, et al., Active parameter control of nonlinear vibrating structures, J. Appl. Mech. (1989) http://dx.doi.org/10.1115/1.3176143.
[43] H. Hertz, Uber die beriihrungfester elastischer korper. (On the contact of elastic solids), J. Reine Und Angewundte Mathernatik 92 (1882).
[44] I.F. Lazar, S.A. Neild, D.J. Wagg., Using an inerter-based device for structural vibration suppression, Earthq. Eng. Struct. Dyn. (2013) http://dx.doi.org/10.1002/eqe.2390.
[45] K. Mnich, et al., Identification of friction in inerter with constant and variable inertance, Meccanica (2022) http://dx.doi.org/10.1007/s11012-022-01547-z.
[46] M. Duncan, C. Wassgren, C. Krousgrill, The damping performance of a single particle impact damper, J. Sound Vib. (2005) http://dx.doi.org/10.1016/j.jsv.2004.09.028.